Millimeter-wave UWB Antenna Design in LTCC Technology

By

Shenario Ezhil A

MASTER OF SCIENCE IN ELECTRICAL ENGINEERING

AT

DELFT UNIVERSITY OF TECHNOLOGY

IRCTR-A-009-08

Millimeter-wave UWB Antenna Design in LTCC Technology

By

Shenario Ezhil Valavan A
Student, Master of Science (Telecommunications), IRCTR

ABSTRACT

Antennas form an integral part of the UWB radar systems which are becoming more popular in numerous safety and security applications. In many cases such radar systems require large UWB antenna array capable of radiating short EM pulses. The focus of this thesis is to develop a differentially-fed transient element for a UWB antenna array operating in the mm-wave frequencies, to be realised in LTCC technology. Theoretical analysis of carried out prior to the final antenna design of three candidate antennas viz. Vivaldi, Stacked Patch and the Shielded butterfly antenna considered suitable to meet the demands, demonstrated that the stacked patch antenna is probably the best candidate for the requirement. However, the use of LTCC, which inherently uses substrates with high dielectric permittivity and differential feeding at mm-wave frequencies are two major challenges for achieving an ultra-wideband operation. These challenges have been successfully overcome and wideband characteristics achieved with the novel antenna design presented in this thesis. The antenna utilizes a coupling aperture, which is differentially fed in substrates with high dielectric permittivity achieving a wide bandwidth of operation. These aspects collectively account for the novelty in the design. The antenna achieves an operational bandwidth of 12.8 GHz with a central frequency of 61.8GHz and front-to-back ratio (FBR) of 12.3 dB. It also has good impedance matching (VSWR<2) over the operating bandwidth. The antenna to be manufactured in LTCC technology can be directly integrated with RF chips on LTCC substrates. An alternative design with an unbalanced feeding structure has been worked out and optimized to meet the initial specifications as well. The single antenna element developed in this thesis project can also be implemented in array to be used in UWB noise radars for imaging applications. The transient UWB operation further aids in achieving high down and cross-range resolutions which are pivotal for applications such as through-dress imaging and concealed weapons detection.

Thesis Advisor: **Prof. Alexander Yarovoy**

ACKNOWLEDGEMENTS

I wish to thank Prof. Alex Yarovoy and Prof.L.P.Lightart for providing me the opportunity to work on this fantastic design project. I thoroughly enjoyed every bit of the experience and challenge, whereby I learnt a lot about practical antenna design. The experience has rekindled my interest in physics and RF. It has motivated me to delve deep into the field of Applied Electromagnetics, which has always been one of the most challenging and defining fields of research in the modern era.

I would like to thank Bill Yang for his excellent mentorship and guidance during the course of the thesis project. I would also like to extend a very special thanks to D.P.Tran, for his practical insights in antenna design, which were pivotal throughout the design stage. I also thank other members of Prof. Yarovoy's UWB group for helping me on various occasions.

Finally, I thank my mom, Sathya, my family and friends for supporting and encouraging me throughout the course of my Masters here in Delft. Without these wonderful people around me, I wouldn't have achieved my goals so far. In a very special way I would like to dedicate this work to my amma.

Shenario Ezhil A

April 2008, Delft

CONTENTS

FIGURES

TABLES

1

INTRODUCTION

Ultra Wideband is a potentially revolutionary technology. It has a wide range of applications in communications, imaging, radar etc,. It is based on the transmission and reception of pulses which are compressed in time, in contrary to the conventional way of using sinusoidal waveforms compressed in frequency. This results in achieving wider bandwidths of operation. Typically the pulses have periods in the scale of nano-seconds. Ultra Wideband is defined by the Federal Communications Commission (FCC) as any technology which occupies greater than 500MHz of bandwidth or alternatively a fractional bandwidth of 20%.

The possibility of a widespread deployment of this technology has sparked a huge interest in this subject among researchers world wide. The power level mask which is authorised by the FCC means that every dB counts in the UWB system. Hence, an effective UWB antenna is critical to the UWB system on the whole. A typical UWB pulse in time domain and its corresponding spectrum is shown in Figure 1.1. Compared to the conventional narrowband technologies, the UWB technology is less vulnerable to narrowband interference due its wide bandwidth.

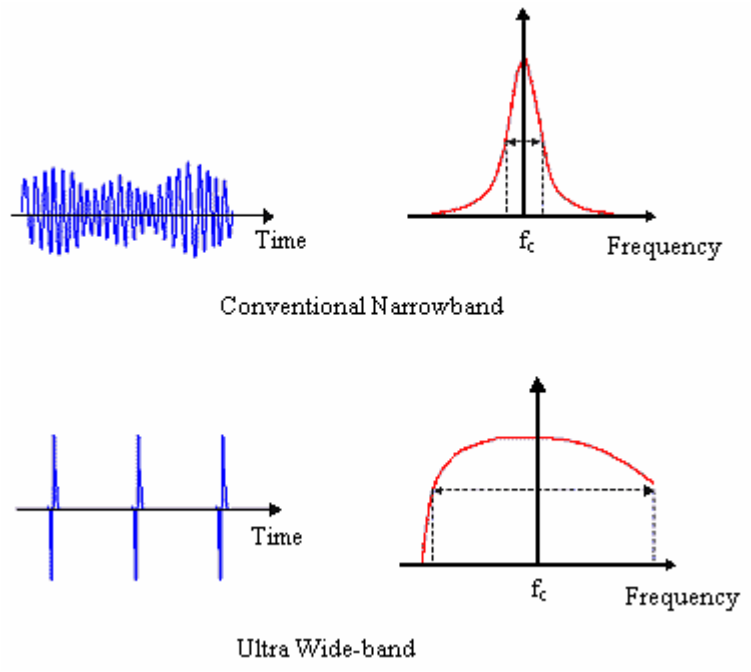

Figure 1.1: Comparison between narrowband and UWB operations in time and frequency domains

1.1 Research Area

The area of research for the Master thesis is concerned with the design of a UWB antenna operating at mm-wave frequencies, to be used for imaging radar applications. The unlicensed wideband at 60 GHz enables short range operations at high data rates. A wide variety of antenna designs for various applications have been proposed in literature. However, the design and implementation of the UWB antennas presents many challenges in itself.

1.1.1 Challenges in UWB Antenna Design

Over the years wideband operations have usually been achieved by having a series of individual narrowband channels over the entire frequency band of operation. Some of the modulation techniques, for example OFDM, are less vulnerable to antenna variation than others. A UWB system, especially for impulse radio, requires an antenna which is capable of receiving all frequencies at the same time instant. Hence, the antenna's behaviour should be consistent and predictable across the operating frequency band. Pattern and matching of the antenna should also be stable across the entire band [1]. A non-dispersive behaviour of the antenna is an important requirement which the UWB antenna needs to satisfy. In the absence of this kind of behaviour, if the dispersion occurs in a predictable manner then it can be compensated for. This makes it more important to concentrate on the phase centre of the antenna apart from the gain and return loss characteristics. This is because

gain is a scalar quantity and thus does not provide any information on the phase variations that might have a serious impact on the UWB antenna's operation. The phase centre may, for instance, vary as a function of frequency or look-up angle, which in turn results in a dispersed waveform.

Dispersion presents an obstruction for multi-band systems as well as those where the radiated signal occupies the entire bandwidth. If an antenna behaves differently at different look-up angles or frequencies then the UWB system needs to compensate for these differences. This compensation is very complicated and also does not ensure that the performance of the dispersive antenna may be equal to that of a non-dispersive antenna [2]. An example for a dispersive antenna is the log-periodic antenna where the large scale components radiate low frequencies and the smaller components radiating the higher frequencies. This results in a chirp like waveform as shown in Figure 1.2. By contrast, a small element antenna like the elliptical dipole antenna radiates a more compact non-dispersive waveform similar to the derivative of a Gaussian pulse, as shown in Figure 1.3. Hence, small element antennas are preferred as it would be compact apart from being non-dispersive.

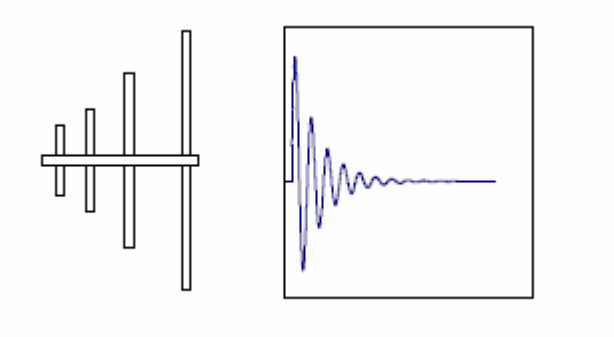

Figure 1.2: Log Periodic antenna and its waveform

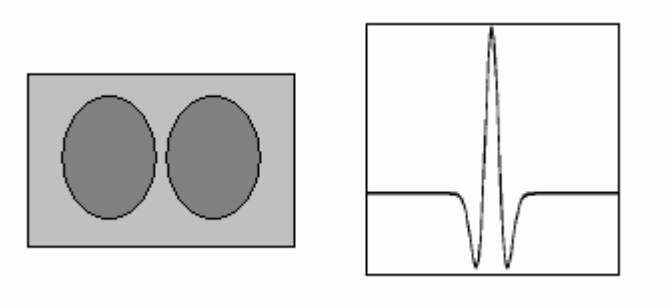

Figure 1.3: Elliptical Dipole and its waveform

UWB antennas at mm-wave frequencies have been designed and implemented of-late for various applications ranging from imaging to communications. The sizes of these antennas are naturally small as the operating frequencies are usually more than 50 GHz. This helps in reducing the problems of dispersion as mentioned above. However, the phase characteristic needs to be studied in order to be sure about the vulnerability of these antennas for dispersion.

1.1.2 Research Problem and Goal of the Thesis

UWB antennas in the mm-wave frequency range have been mostly implemented in PCB technology. Further, the use of MMIC's in modern applications provides a differential output which needs to be used as the input for the antennas. This in turn requires a differential feeding structure for these antennas. A differential feeding structure ensures that the unnecessary losses due to the use of BALUN for feeding unbalanced antennas are absent. Conventional feeding schemes result in losses which need to be compensated for separately. Further, the design of these antennas in LTCC technology, which inherently uses substrates with higher permittivity, presents a bigger challenge with respect to the achievable bandwidth. The inverse relation between the permittivity and the achievable bandwidth implies that achieving a wider bandwidth needs intuitive designs which annul the effect of the higher permittivity. However, the fabrication in LTCC technology has certain advantages compared to the conventional PCB technology. Apart from being cheaper compared to the PCB, the LTCC technology aids in the fabrication of multilayered structures. This is due to the inherent design procedure of the LTCC technology where the fabrication is done in a layered manner. The design of a UWB antenna at mm-wave frequencies in LTCC technology is precisely the topic of research in this thesis. The thesis project is part of the larger RADIOTECT project sponsored by the EU. The antenna also needs to be planar in order to be used in an array configuration as part of the future work in the RADIOTECT project.

The required characteristics of the antenna with respect to important parameters are presented in Table 1.1.

Parameter	Requirement
Frequency range	60-70 GHz
Gain	+5 to +10dB (At least a positive gain over the bandwidth)
Beamwidth	~ 100 to 120 Degrees (both E and H planes)
Size	Less than 2 cm
VSWR	Less than 2 over the bandwidth
Front to Back Ratio (FBR)	15 – 30 dB
Feeding	2*50 Ω Differential Feeding

Table 1.1: Required characteristics of the antenna

1.2 State of the Art in UWB Antennas

UWB systems transmit and receive ultra short pulses in time domain, in other words they use a wideband with low power transmissions. This is primarily the reason for employing UWB mostly in short range applications. The use of ultra short pulses increases the difficulty of detection and interception, which was the main reason for UWB to be mainly used in military purpose alone for decades. The end of the cold war, followed by a rapid progress in telecommunication technologies paved the way for the application of the UWB technology for commercial use. In 2002, the Federal Communications Commission (FCC) specified the technical standards and the operational restrictions for three types of UWB systems (vehicular radar systems, communications & measurement systems and imaging systems).

Although most of the current research work has been focussed on omni-directional UWB antennas there has also been considerable interest in directional antennas. The first class of UWB antennas are mostly used in wireless communications, mobile devices etc, whereas the latter in radar and imaging applications.

Before the 1990's, most of the UWB antennas proposed were based on the general volumetric structures. Today though, the state of the art of UWB antennas focuses on Microstrip, slot and planar monopole antennas with different matching techniques to improve the bandwidth ratio without loss to its radiation properties [3].

In the past, one of the serious limitations of the Microstrip antennas was its narrow bandwidth characteristics compared to the other types of antennas. This limitation is successfully dispensed by increasing the matching impedance bandwidth ratio by increasing the size, height, volume or feeding and matching techniques.

Several Microstrip UWB antennas for wireless applications, imaging and mobile devices have been proposed. A coplanar waveguide (CPW)-fed planar UWB antenna [4], having a small size and frequency band notch for wireless local area network (WLAN) frequency of 5.25 GHz, adjustable by varying the length of the V-shaped slot, is shown in Figure 1.4. The frequency bandwidth is approximately from 2.8 to 10.6 GHz. A UWB slot antenna realised in LTCC technology is shown in Figure 1.5. The antenna can share the ground plane with other radio circuitry. The radiating element has an elliptical shape. The impedance bandwidth is from 3 to 10.6 GHz with a quasi-omni-directional radiation pattern at lower frequencies. A similar design was also published, but in this case, it is a printed circular disc monopole UWB antenna (Figure 1.6). This design has the ground plane and the radiating structure in the same plane, suitable for integration with printed circuit boards. The impedance bandwidth is from 2.78 to 9.78 GHz with an omni-directional radiation

pattern. A comparison of the antennas discussed here along with the well known UWB antenna types is shown in Table 1.2.

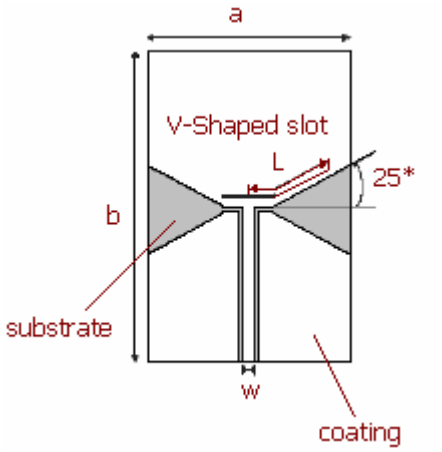

Figure 1.4: CPW-fed Planar UWB antenna with frequency band notch function

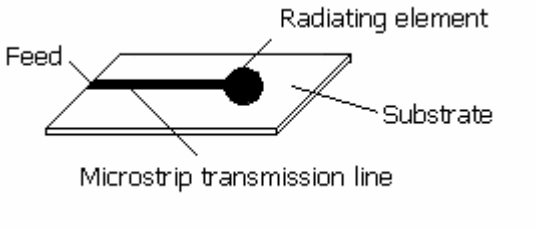

Figure 1.5: UWB Slot antenna

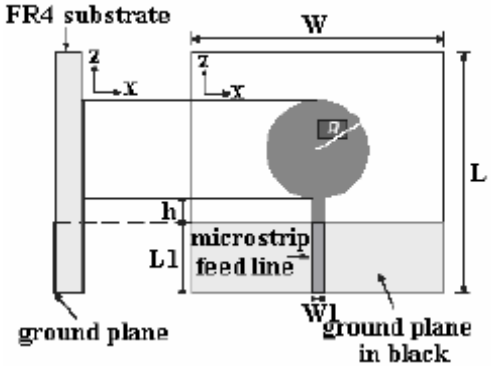

Figure 1.6: Printed circular disc UWB Monopole antenna

Antenna Type	Gain	Feed	Size	Bandwidth	Main Features
Vivaldi	--	Balanced	150x120mm	Theoretically unlimited	Requires broadband Balun
Rectangular patch	Up to 5dBi	Unbalanced	15x14.5mm	3.2-12GHz	Substrate ε_r=4.4
CPW-fed planar with frequency band notch function	Up to 5dBi	Unbalanced	22x31mm	2.8-10.6GHz Notch band 5.15-5.35GHz	Substrate ε_r=4.4
LTCC UWB slot antenna	--	Unbalanced	11x17mm	3-10.6GHz	LTCC technology
Printed circular disc monopole antenna	--	Unbalanced	42x50mm	2.78-9.78GHz	Substrate ε_r=4.7
Frequency notched UWB microstrip slot antenna with tuning stub	Up to 5dBi	Unbalanced	48x41mm	2.66-10.76GHz	Substrate ε_r=2.65
Bi-arm rolled monopole antenna	Up to 9dBi	Unbalanced	16x3mm	3.1-10.6GHz	Smallest size
Square planar monopole antenna using notching technique	4-6dBi	Unbalanced	30x30mm with Ground plane	1.97-12.73GHz	Wider matching impedance bandwidth
Rectangular planar monopole antenna using bevelling technique	5-7dBi	Unbalanced	60x39mmwith Ground plane	1.65-20GHz	Widest matched impedance bandwidth

Table 1.2: Comparison of UWB antennas

1.3 Approach Methodology

The project's development is broadly divided into three main phases, with each phase having respective milestones. The first phase essentially has three sub-stages. First, the literature survey of the materials related to the mm-wave antenna design is carried out. Next, each of the candidate antennas viz. the Vivaldi antenna, the Stacked Patch antenna and the Shielded Butterfly antenna is theoretically analysed with respect to the performance metrics specified in Table 1.1 in Section 1.1.2. Numerical models of the three candidate antennas are modelled in FEKO with the specifications presented in the respective publications. This study provides a good insight into the performance which can be expected from these antennas. The choice of the type of antenna is made based on the performance comparison of the individual antennas with respect to the main performance metrics, the use of a differential feeding structure and realisation challenges in LTCC technology.

The second phase involves the design of the antenna configuration and the subsequent optimization of the antenna's dimensions for optimum performance. This phase also includes tests for the antenna's phase characteristics, time domain ringing etc., which is very pivotal for Ultra-Wideband operations and the subsequent signal processing. The numerical modelling is done in CST. The third phase concerns the design modifications which need to be done for the antenna to be realised in LTCC. This is followed by the realisation of the antenna and an experimental verification of the antenna's characteristics.

1.4 Thesis Contributions

The main contribution of this thesis is the design and implementation of a UWB antenna operating at mm-wave frequencies, which will be used for UWB noise radar for imaging applications. This thesis provides a broad overview of the types of antennas which are considered as candidates for the main design. A comprehensive description of the design of the final antenna and the challenges in LTCC technology are also presented. The designed antenna is well suited for short range imaging applications, for example in airports, due to its wide beamwidth. The antenna also employs differential feeding which aids in using it with a MMIC, a fact which is indispensable in many modern applications. Further, the antenna's planar structure and an almost static phase center imply that it can be readily used in array configurations.

Novelty in the Antenna Design

The coupling aperture of the H-Shaped Aperture Coupled Stacked Patch Antenna, presented in this thesis, is **differentially fed** with cylindrical feeding probes. The antenna design proposed, apart from being simple also achieves a wideband of operation and good radiation characteristics at the **mm-wave frequencies** in substrates with **high dielectric permittivity** (ε_r=7.4) compared to the conventional designs which normally use substrates with lower permittivity values. The use of differential feeding at mm-wave frequencies and substrates with high dielectric permittivity are the features which collectively account for the novelty in the antenna design presented in the thesis.

1.5 Overview of the Report

The introduction is followed by a description of the LTCC fabrication process, presented in Chapter 2. A detailed review of the analysis of the candidate antennas is presented in Chapter 3. The analysis and results obtained from two types of Stacked Patch antenna configurations which were tested prior to the final design are presented in Chapter 4. Chapter 5 presents a detailed explanation, analysis and the simulated results of the Aperture Coupled Stacked Patch Antenna with differential feeding. Conclusions and suggestions for future work are given in Chapter 6. A brief explanation of the numerical methods employed is provided in Appendix A. The references which contributed to the intuitive understanding and the subsequent designing of the antenna are listed at the end of this report.

2

LTCC TECHNOLOGY and ANTENNAS

2.1 A Basic Introduction

Low Temperature Co-fired Ceramic (LTCC) is a multilayer platform technology that is used in fabrication of components, modules and packages in wireless, automotive, military, medical and several other areas. LTCC enables the integration of passive components, such as filters and antennas with active components in the same package for applications ranging up to millimeter-wave frequencies. Components can be placed in different layers (even up to 70 layers), and three-dimensional integration enables miniaturization of modules. LTCC processing enables cavities and conducting 'vias' to be placed inside the substrate. Major benefits of LTCC are low conductor and dielectric losses, good thermal conductivity, stability, hermeticity and cost efficiency. However this technology has disadvantages with regard to the fabrication tolerances at millimeter-wave region

2.2 Fabrication Process

The LTCC package is formed by layered dielectric glass/ceramic sheets or tapes over which the metallization is manufactured using the screen-printing or photo-imaging technologies. The LTCC fabrication process is described in Figure 2.1. First, via holes are punched in the "green"

glass/ceramic sheets. Then, via holes are metalised to form electrical interconnection between layers. This is followed by the fabrication of electrical conductors and passive components on each glass/ceramic sheet separately. The different layers are aligned and laminated. After lamination, the ceramic sheets are co-fired or sintered together with conductors. Finally, the circuits are separated. Sometimes the etched conductors can be post-fired on the top after the LTCC processing. In LTCC, glass/ceramic substrates have sintering temperatures below 900 °C while the alumina substrate used in HTCC (High Temperature Co-fired ceramic) requires a temperature of 1600 °C. Low sintering temperature of LTCC enables co-firing of substrate with gold and silver conductors which have melting points 960 °C and 1100 °C, respectively.

When compared to conductors with high melting point, such as tungsten or molybdenum, used in HTCC, silver and gold have higher conductivities which result in a lower conductor loss in LTCC [4]. During the sintering, the ceramic sheets shrink because of the binding of ceramic ingredients near the sintering temperature. There are two co-firing methods that are used in practice: 1) free sintering and 2) zero-shrinkage. Shrinking has to be taken into account in the LTCC process. Exact values of shrinking of the glass/ceramic sheets and metallization are quite difficult to predict because of the lack of processing repetitions. Especially, as conductor widths or spacing are in the order of the minimum values that can be processed, the prediction of the realised dimensions of the structures becomes even more difficult.

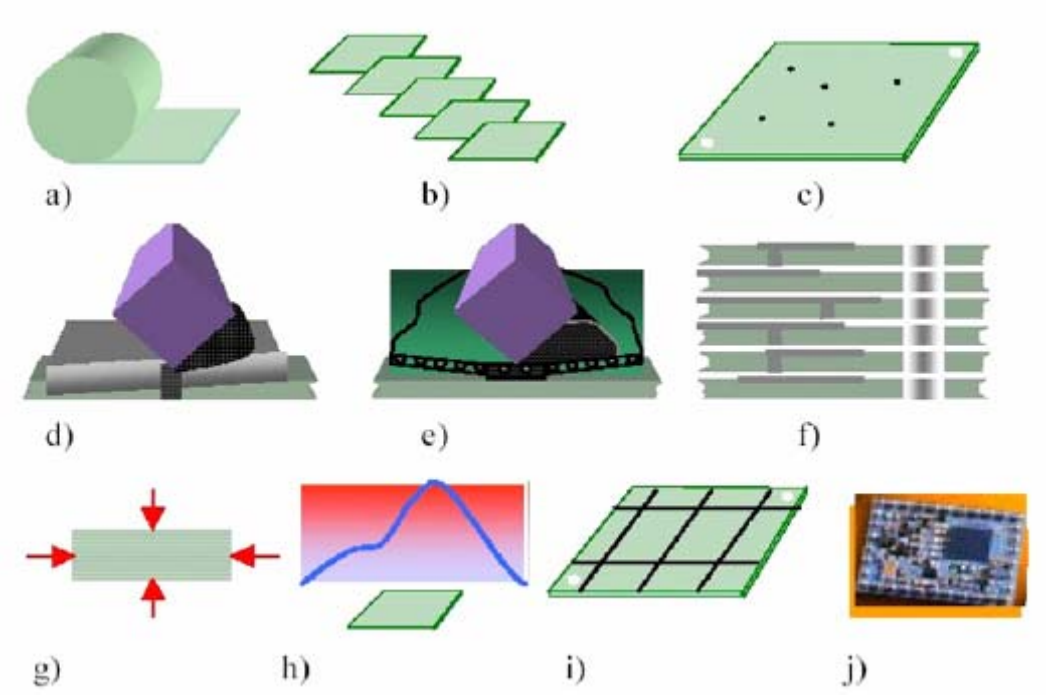

Figure 2.1: The LTCC process: a) glass/ceramic LTCC tape material, b) tape blanking, c) via punching, d) via metallization, e) conductor printing (or photo-imaging), f) layer alignment and stacking, g) lamination, h) interring, i) dicing of fired panel, j) component and die attach. (Courtesy – VTT Electronics) [3].

2.3 LTCC materials

Several commercial LTCC tapes are available for high-frequency applications. Traditional materials can be used in free-sintering up to millimeter-wave frequencies. With more advanced materials the zero-shrinkage processing is possible. Material information of the commercial LTCC tape systems is presented in [5]. For this project, the material with dielectric permittivity of 7.4 and loss tangent equal to 0.002 was used for the fabrication process. The material has low losses and a stable dielectric permittivity value at mm-wave frequencies. The thickness of each layer is 125 μm, which becomes 104 μm when co-fired (Appendix C).

2.4 UWB antennas in LTCC

In this Section, the literature concerning recent works on LTCC antennas and arrays is briefly discussed. LTCC is well-suited for fabrication of planar structures. Microstrip antennas are widely used at microwave and millimeter-wave regions. Recently, Vivaldi antennas have been realised in LTCC technology which have an extremely wideband of operation. Theoretically, the Vivaldi antenna has an infinite bandwidth; the only limitations are its physical size and fabrication capabilities. The practical limitation for the bandwidth is the Microstrip-to-slotline transition. The only solution for this problem is the use of a wideband balun. An antipodal Vivaldi antenna with a 60% operational bandwidth is presented in [8].

Apart from these, there are also other Stacked Patch antenna configurations realized in LTCC technology. The design in [12], presents a Stacked Patch configuration with an embedded air cavity, which achieves around 18.5% bandwidth. The main use of this antenna is in short range imaging. A Stacked Patch antenna configuration presented in [13] is used for wireless application in the 40GHz frequency range. Both the single element and array implementations are presented. Due to poor gain of the patch, usually several antenna elements are laced in an array. An 8x8 model has been realised in LTCC at 40GHz to be used for the Impulse Radio applications [14]. The state of the art with respect to UWB antennas in LTCC as of now is limited.

All the three candidate antennas considered in this project, have been implemented in LTCC with acceptable performances. But the scope for improvement remains large, especially with the LTCC technology where the use of higher permittivity substrates is an essential requirement. This requirement presents a big challenge for achieving wideband operations and also causes other problems like the increase in the amount of surface waves when thicker substrates are used. Techniques to annul the effect of the higher permittivity substrates need to be incorporated along

with the antenna design. With a growing interest in LTCC technology, it is evident that more intuitive and defining publications will be presented in the near future.

3

ANALYSIS OF CANDIDATE ANTENNAS

The analysis of the antennas involved a feasibility study for each of the candidate antennas with respect to the requirements of the project. The analysis is done with a special emphasis on the usage of a differential feeding structure and the realisation issues in LTCC. Some related antennas were studied from recent publications. The basic models of all the candidate antennas were also implemented in FEKO and the results obtained are used to decide on the final candidate antenna for the design and optimization. The description of the individual antennas viz. the Vivaldi, Stacked Patch and Shielded Butterfly and their corresponding simulation results from FEKO are presented. A comparative study of the three antennas and the basis for the selection of the final antenna is presented in the end of this chapter.

3.1 Vivaldi Antenna

The Vivaldi antenna is a well known wideband antenna which is used in systems which require a very wide bandwidth of operation. The antenna, first proposed by P.J. Gibson in his 1978 paper [7] has been modified over the years according to various requirements. A Vivaldi antenna providing a 60 % operational bandwidth realised in LTCC technology is presented in [8]. A novel technique to reduce

the asymmetric phase distribution between the two wings by decreasing the effective permittivity of the medium using punctured holes is also presented in [8].

From the publications which deal with the realisation of the Vivaldi antenna in LTCC, the performance characteristics of the Vivaldi antenna with respect to the main parameters can be summarised as follows. The Gain of the Vivaldi is positive through out the entire bandwidth of operation. A gain of +5dB and +5 to +10 dB over the entire bandwidth is reported in [8] and [9] respectively. A beam-width of around 80 to 100 degrees in the E-plane along with a front to back ratio (FBR) of 10 to 15 dB is reported in both [8] and [9]. The size of the realised antenna in LTCC is under 10 mm in [8] and 25 x 50 mm in [9]. These characteristics look very promising as they satisfy most of the requirements of the project. Nevertheless, issues regarding the feed for Vivaldi remain a challenge.

Connecting the feed directly to the antenna makes it insensible to fabrication tolerances, a fact which is indispensable, especially in LTCC technology. By doing so, the influence of the feed on the radiation pattern is also minimized. But, the design of a balanced feed is very tough for the Vivaldi, as we require a wideband BALUN, which influences the performance of the antenna too. Implementation of differential feed for the Vivaldi antenna has not been studied extensively so far.

Apart from this, there are other factors which are quite challenging. From [10], it is clear that the mathematical description of the taper opening has to be more complex than mere exponential functions to achieve the required design goals. Another well known problem with the Vivaldi is the increase in the back radiation at lower frequencies. Further, there is a lack of use of Vivaldi arrays in the frequency band of interest (60-70GHz).

3.1.1 Implementation of Vivaldi Antenna in FEKO

The Vivaldi design implemented in FEKO was slightly different from the one given in [9]. Modifications were made to test the use of the differential feed for the Vivaldi aperture. The antenna simulated in FEKO is presented in Figure 3.1. The dimensions of the antenna are 25 x 50 x 0.8 mm. The test was done with two flares, one on top of the substrate and another on the other face of the substrate material. The specifications for the flare are the same as given in [9]. The feeding was provided using an edge port feed with a 1 V power supply. The upper patch was connected to the positive and the lower patch to the negative of the edge port. The performance of the antenna with respect to the main parameters such as gain, impedance, VSWR and beam-width are captured in the plots presented in Figure 3.2 - 3.5.

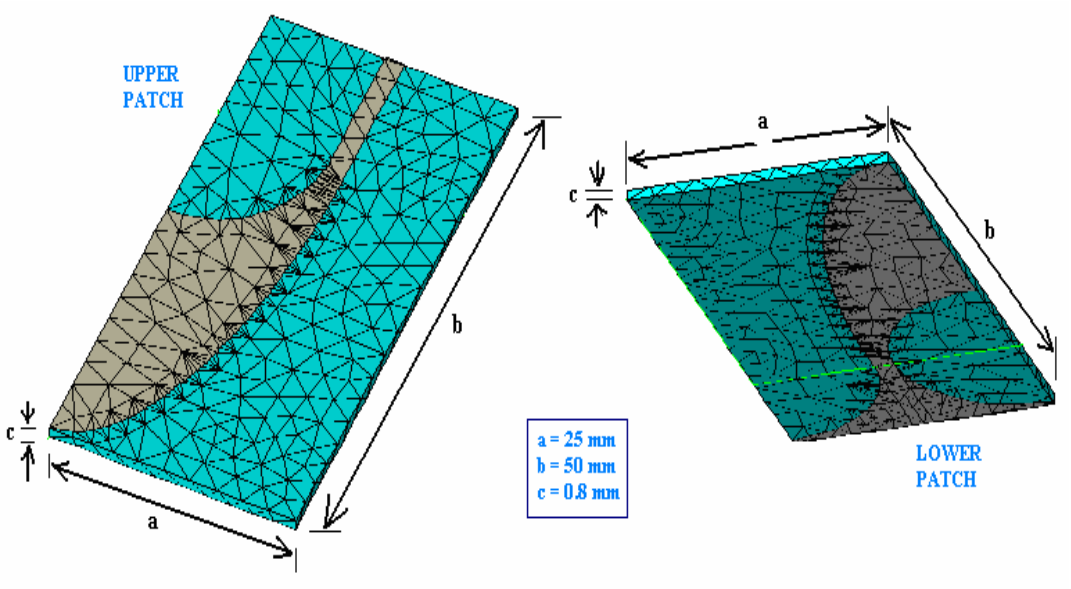

Figure 3.1: Simulated Vivaldi antenna in FEKO

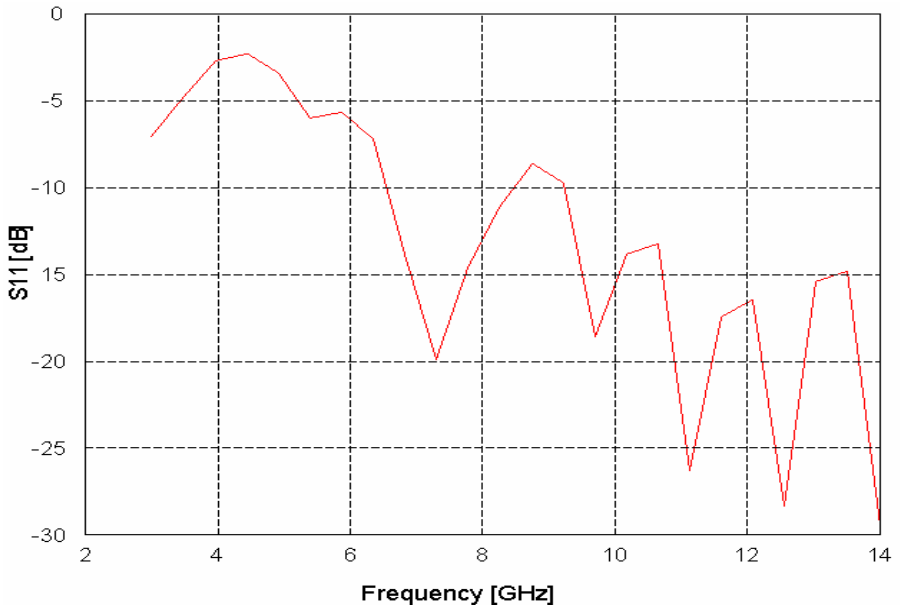

Figure 3.2: S_{11} – Impedance plot of the simulated Vivaldi antenna

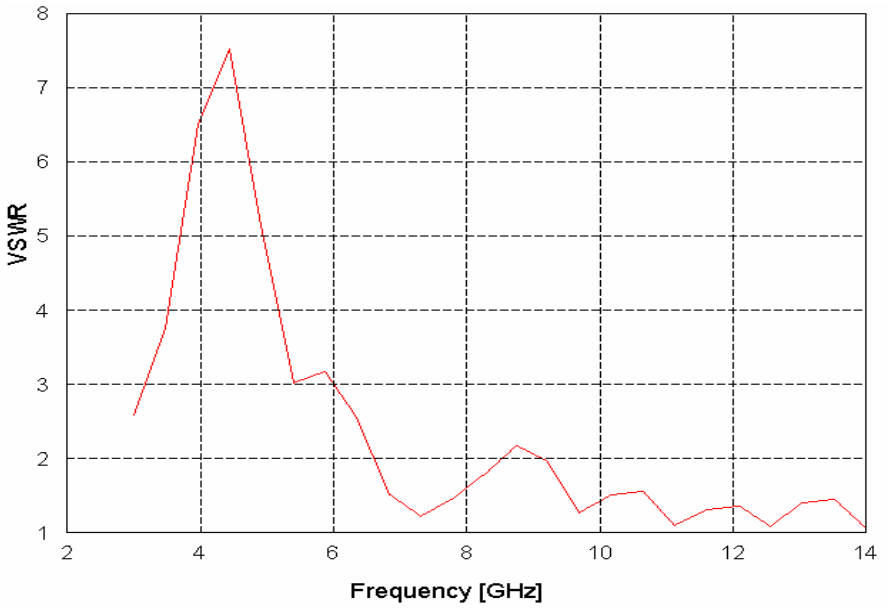

Figure 3.3: VSWR characteristics of the simulated Vivaldi antenna

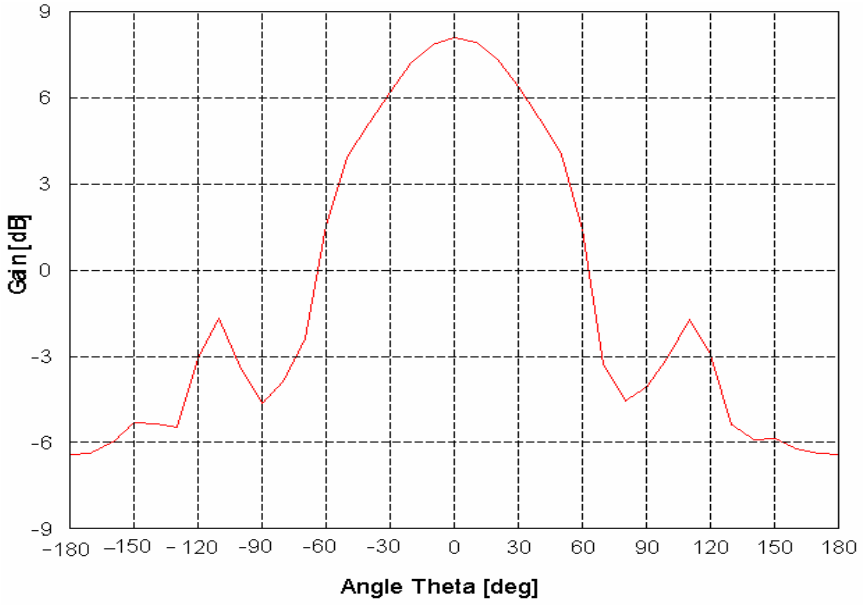

Figure 3.4(a): Gain characteristics of the simulated Vivaldi antenna at 10.6 GHz

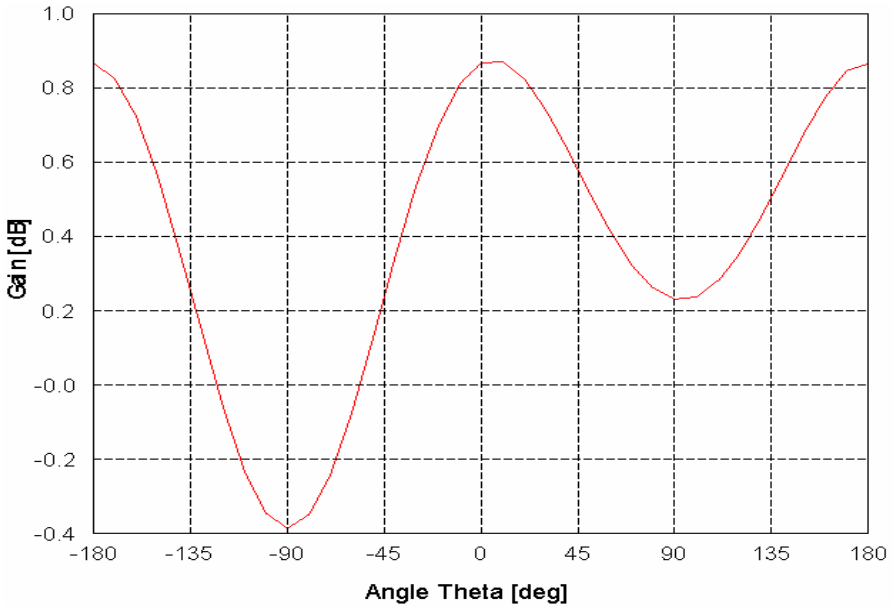

Figure 3.4(b): Gain characteristics of the simulated Vivaldi antenna at 4.7 GHz

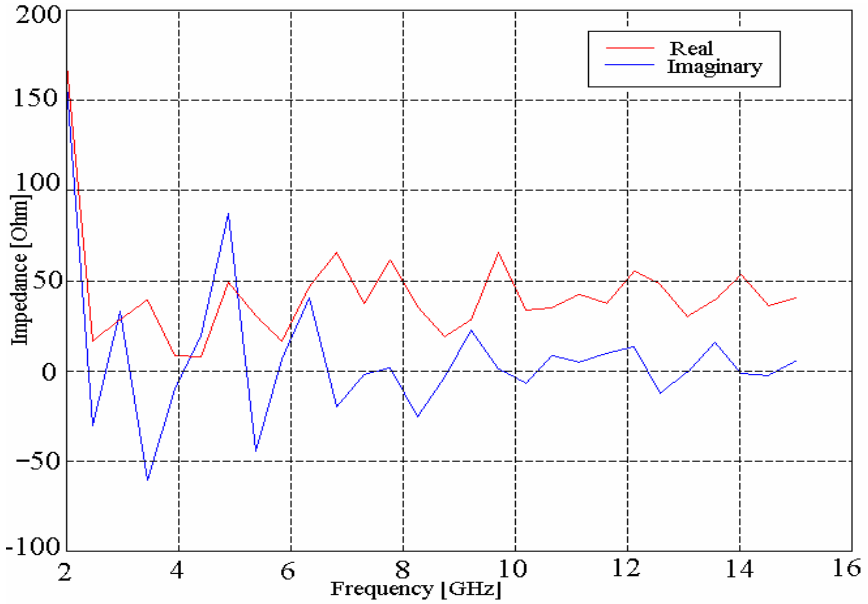

Figure 3.5: Impedance plot of the simulated Vivaldi antenna

From the plots shown in Figure 3.2 and 3.3; it is clear that the antenna implemented in FEKO has an operating bandwidth which is larger compared to the antenna model presented in [9]. There is however a small deviation from the normal operation around 8.75 to 9.25 GHz. In relation to this fact, we can also notice from Figure 3.5, that the imaginary part shows peaks in the frequency range

simulated. This can be attributed to the fact that the feed may not be properly matched to the antenna. This is because the antenna was fed using an edge port, which is a highly simplified version of the usual feeds used for a Vivaldi antenna. Publications which concentrate only on the feeding techniques indicate the vitality of having a proper feeding, especially for the Vivaldi structure, which requires the design of a wideband BALUN due to its larger bandwidth of operation. The gain characteristic at 10.6GHz is shown in Figure 3.4(a). From the graph it can be observed that the front to back ratio (FBR) is a level of 10 dB. However, at low frequencies of operation, the Vivaldi antenna radiates almost equally in both the forward as well as the backward directions, which is clear from Figure 3.4(b). This is a serious concern as the use of MMIC's in the antenna's rear, as required in the project's specifications, may damage the integrated circuits.

The characteristics of the simplified Vivaldi antenna implemented in FEKO provide a good conformance with respect to the main parameters. Further, the Vivaldi antenna design in LTCC presented in [8] has been implemented in the frequency range of 60 – 100 GHz. This ensures that the realisation of the antenna will not have any unknown challenges except that of the differential feed usage.

3.2 Stacked Patch Antenna

The Stacked Patch antenna is essentially a modification of the conventional patch antenna. The antenna's popularity is mainly due to its simplicity in terms of the design and implementation. Stacked Patch antennas can achieve a wider bandwidth than the traditional Microstrip antennas and they have also been realised in LTCC used for a variety of purposes. The antenna can provide an operational bandwidth of 7 – 20 %. Typically these antennas have two patches (upper and lower patch), and the radiation is mainly due to the coupling between these two patches. The antenna has evolved from the basic aperture coupled patch antennas described in [12]. It has been used for varied application ranging from communication to breast cancer imaging. The antenna required for this project has to be efficient in terms of the performance metrics, simple in terms of design and also suitable for the planar array implementation. The Stacked patch antenna has features which makes it an attractive candidate antenna.

3.2.1 Implementation of Stacked Patch Antenna in FEKO

The model implemented in FEKO has similar dimensions as given in [13], however with some minor modifications of the length and the breadth of the outer dielectric cube. Instead of the specification of 15 x 20 x 1.17 mm, the model implemented in FEKO has dimensions 8 x 14 x 0.7846 mm. The reduction in the length and breadth of the cube does not have a significant effect on the performance of the antenna. The lower part below the intermediate ground plane of the antenna presented in [13] has been removed as a simplified wire feed is used to feed the lower patch. The transition from the slot to the Microstrip line has also been removed in the model in FEKO. The intermediate plane between the feeding line and the lower patch has been made as the antenna's main ground plane, which is the main difference with respect to the original model. The dimensions of the lower patch, the top patch and the air cavity have not been modified.

A graphical side-view representation shown in Figure 3.6 provides a comparison between the original model [13] and the one simulated in FEKO. It can be noticed that the part below the intermediate ground plane in the original model is dispensed with to make the model simpler for the primary testing procedures. A three dimensional view of the model implemented in FEKO is shown in Figure 3.7.

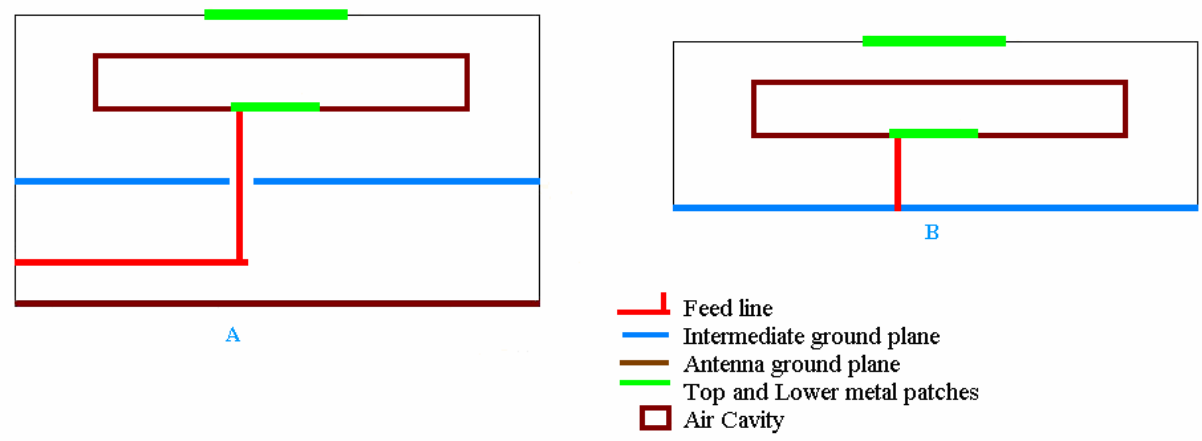

Figure 3.6: Graphical comparison between the original and the model simulated in FEKO A) Actual model B) Simulated model in FEKO

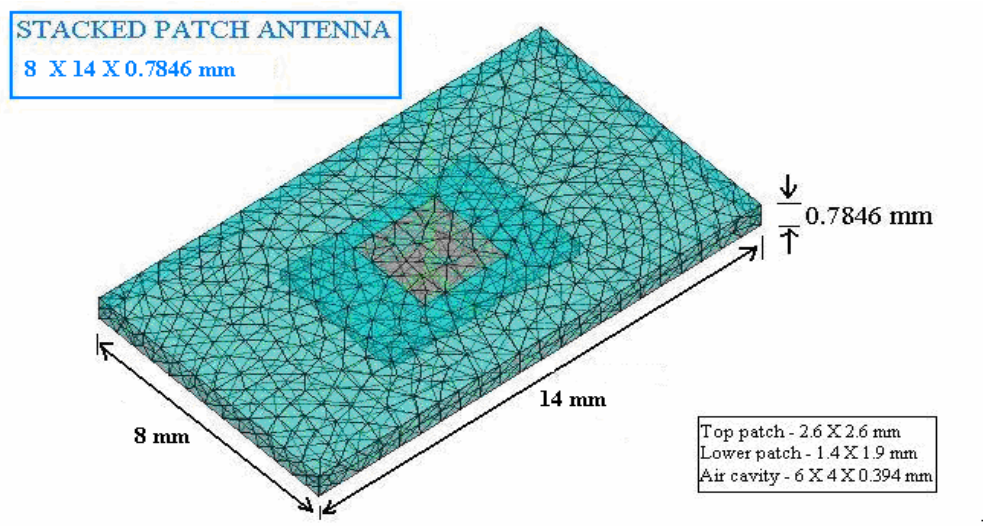

Figure 3.7: Stacked Patch model implemented in FEKO

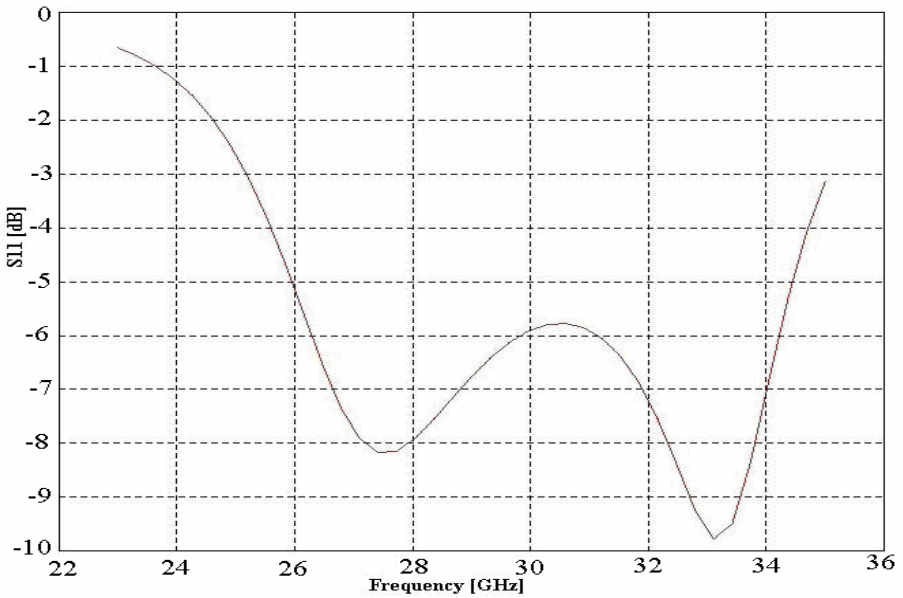

Figure 3.8: S_{11} characteristics of the simulated Stacked Patch antenna

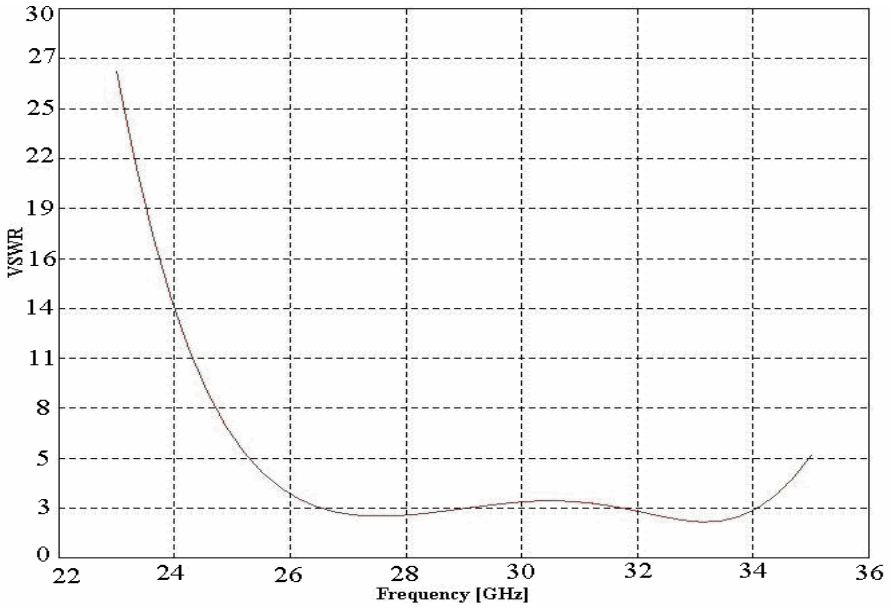

Figure 3.9: VSWR characteristics of the simulated Stacked Patch antenna

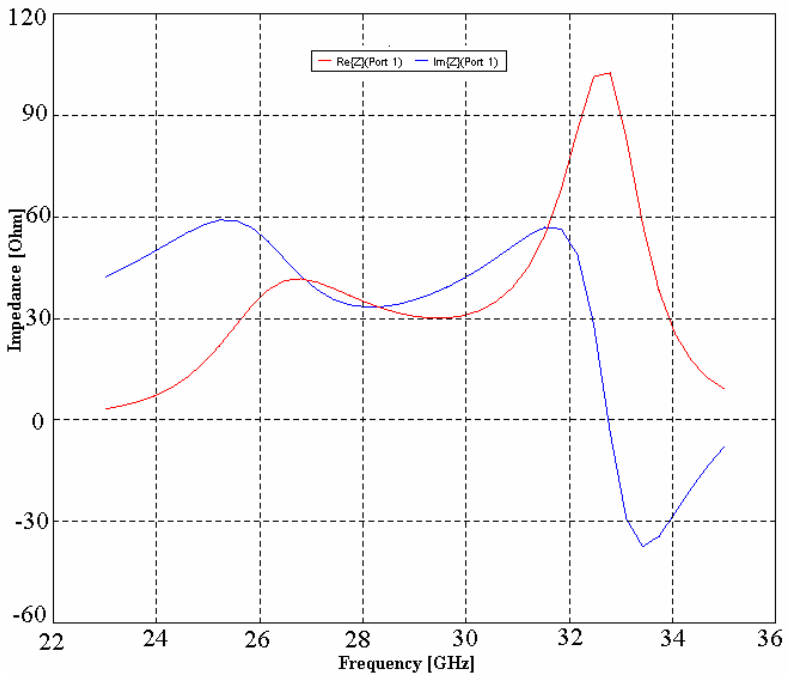

Figure 3.10: Impedance characteristics of the simulated Stacked Patch antenna

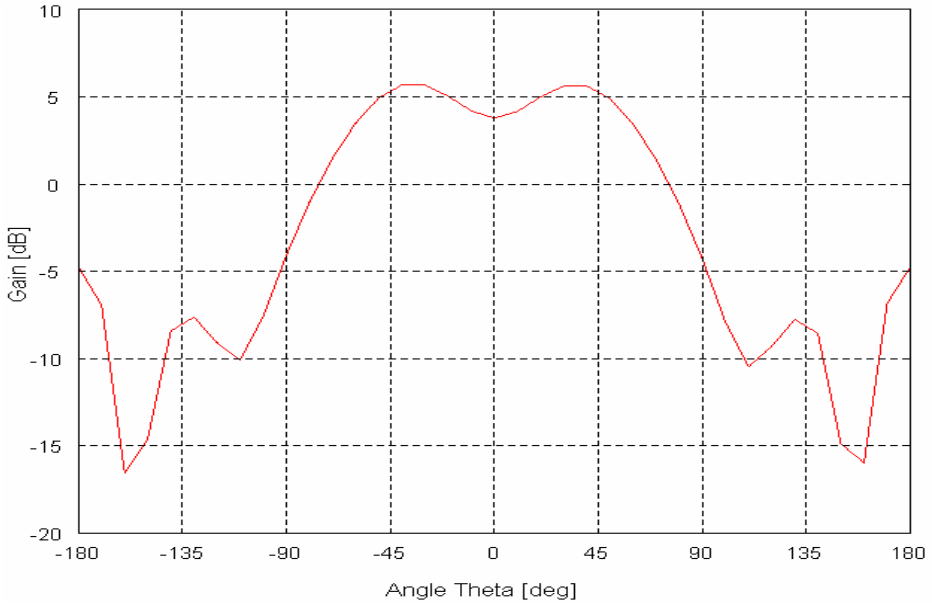

Figure 3.11: Gain characteristics of the simulated Stacked Patch antenna at 27.5 GHz

From the plots in Figure 3.9 – 3.11, showing the impedance characteristics along with the S_{11} and the VSWR provides an insight into the matching obtained for the antenna. It can be inferred from the graphs shown in the Figure 3.9 and 3.10, that the impedance matching obtained by feeding the antenna with the wire port is not sufficient. This deviation can be explained as follows. In the original model [13], the inductive effect due to the feed pin is balanced by the capacitance due to the Microstrip transition and the antenna's intermediate ground plane, which act like the two plates of a capacitor. The lack of this type of a feeding structure and the use of a wire feed can be considered as the main reason for the deviation in the performance characteristics of the antenna modelled in FEKO compared to the original design. The presence of two resonances in the S_{11} plot is however similar to that obtained in [13]. Large values for the imaginary part of the impedance curves can be translated as a lack of proper compensation due to the use of the simplified wire feed which has no provision to compensate for the feed pin's inductive effect. A gain of +5 dB peak is achieved at the center frequency of 27.5 GHz using the simulated antenna model. The front to back ratio (FBR) is nearly 10 dB, which despite being less than the requisite, is at an acceptable level.

The other favourable factors for using the Stacked Patch antenna are that the antenna is comparatively simpler in terms of design and well suited for planar array implementation. Further, it has been presented in other publications that the realisation of this antenna in LTCC will not have any inherent problems on its own. The investigation for the use of differential feeding for stacked path antenna is still in its infancy. Nevertheless, there are related publications of late, which have

delved into this matter. The approach is plausible as similar designs with minor differences have been realised, however at lower frequencies.

3.2.2 Phase Characteristics and Issues of ringing

The phase characteristic of the Stacked Patch antenna is linear over the simulated frequency band of operation from 25 – 32 GHz as shown in Figure 3.12(a). This ensures that the antenna can be used for the UWB based imaging, as the phase linearity is an important requirement for the accurate functioning of the UWB system.

The issue of ringing is another important characteristic which has to be investigated in the case of the Stacked Patch antenna. From the plot shown in Figure 3.12(b), it is clear that there are some ringing pulses after the main pulse, but their level is negligible compared to the main pulse. We can hence conclude that the antenna has an adequate level of performance and hence it is comprehensible that the ringing problem is not a serious issue.

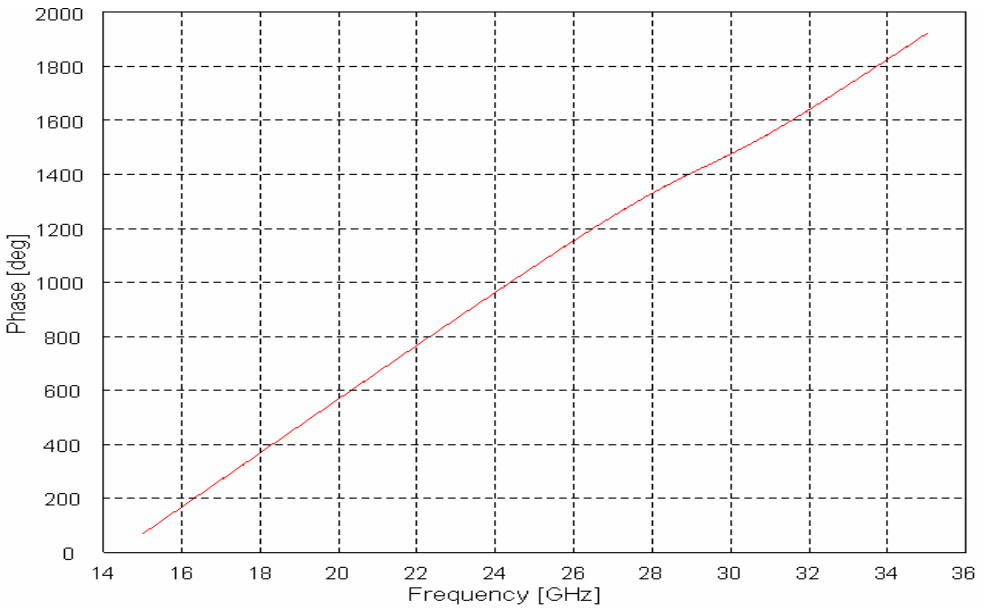

Figure 3.12(a): Phase characteristic of the simulated Stacked Patch antenna

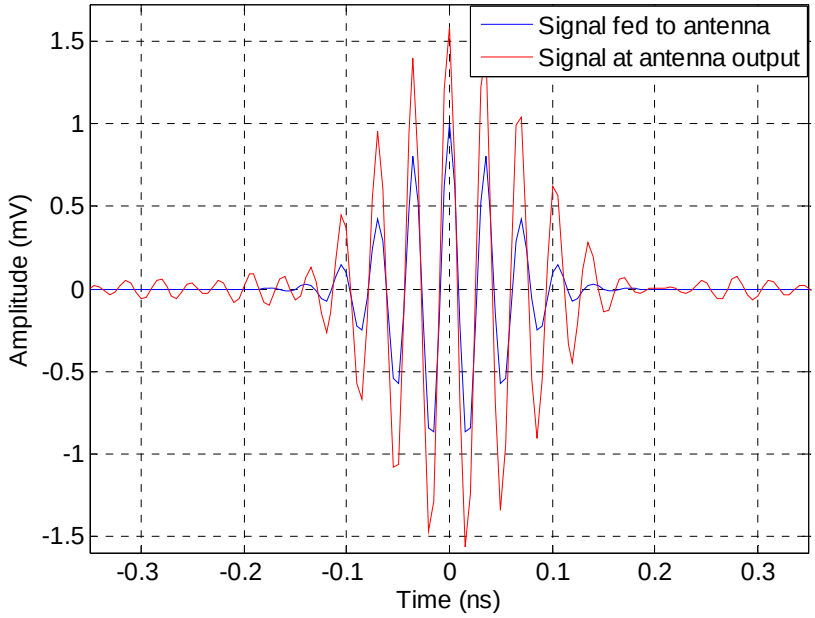

Figure 3.12(b): Ringing characteristic of the simulated Stacked Patch antenna

3.3 Shielded Butterfly Antenna

The Shielded Butterfly antenna is an indigenous design done at IRCTR. The antenna is essentially an extension of the butterfly antenna with elliptical flares, the main difference only being the use of the back shield which has an advantageous influence on the performance. The antenna realised here in IRCTR makes use of the differential coaxial feeding structure operating in a frequency range of 3 to 10 GHz. It has a positive gain over the entire operational bandwidth with a very broad beam-width of around 120 degrees as required for the project. Besides this, the antenna also has a good front to back ratio (FBR) of around 20 dB. The size of the antenna is however large compared to the requirements. The dimension of the antenna which was realised in IRCTR is 50 x 50 x 12.5 mm. The dimensions of the back shield are based on the optimization processes presented in [11]. It is observed that an increase in the length of the shield increases the operational bandwidth and an increase in the height of the shield increases the number of resonant peaks. The influence of the welt on the performance is only minor.

3.3.1 Implementation of Shielded Butterfly Antenna in FEKO

The model implemented in FEKO is shown in Figure 4.13. The model essentially has the same dimensions as the original antenna presented in [11], the only difference being with respect to

feeding. The feeding structure in FEKO is modeled using a wire feed with the voltage source exactly in the middle of the triangular wire segment, which feeds both the elliptical flares. This is done to mimic the differential feeding used in the original antenna.

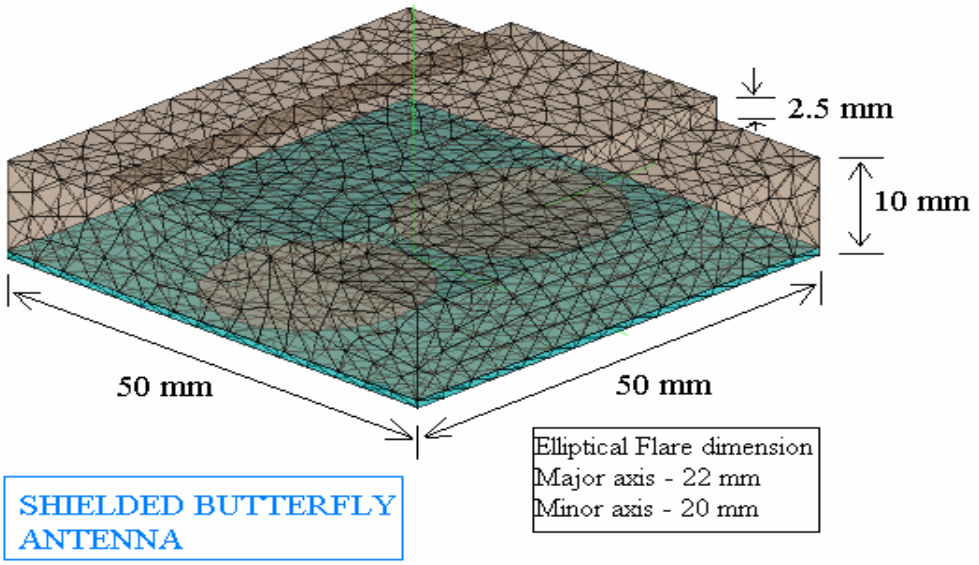

Figure 3.13: Shielded Butterfly antenna model implemented in FEKO

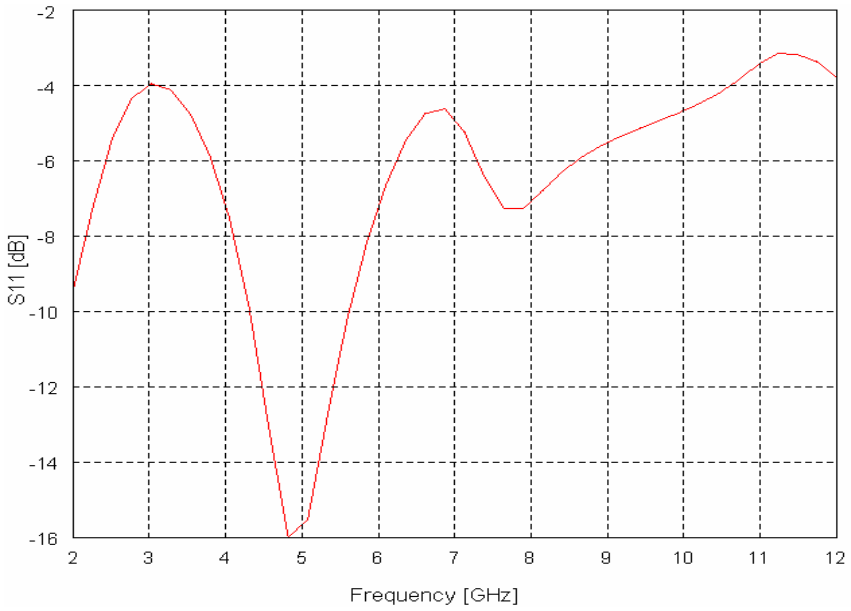

Figure 3.14: S_{11} characteristics plot of the simulated Shielded Butterfly antenna

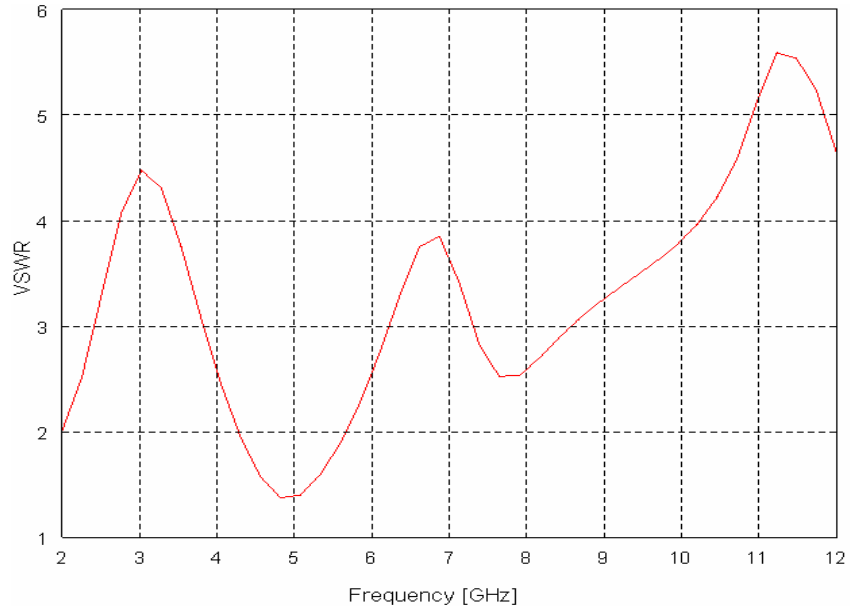

Figure 3.15: VSWR characteristics of the simulated Shielded Butterfly antenna

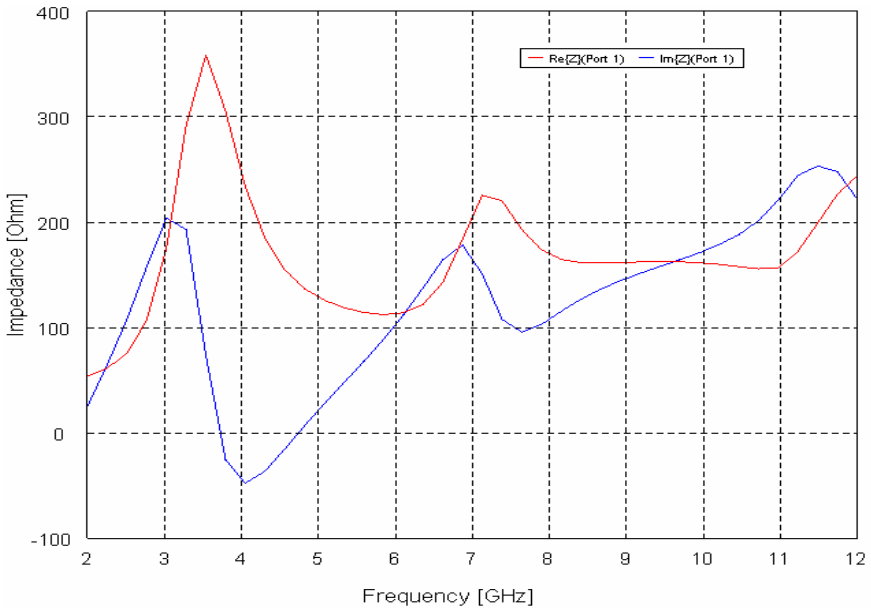

Figure 3.16: Impedance (Z) plot of the simulated Shielded Butterfly antenna

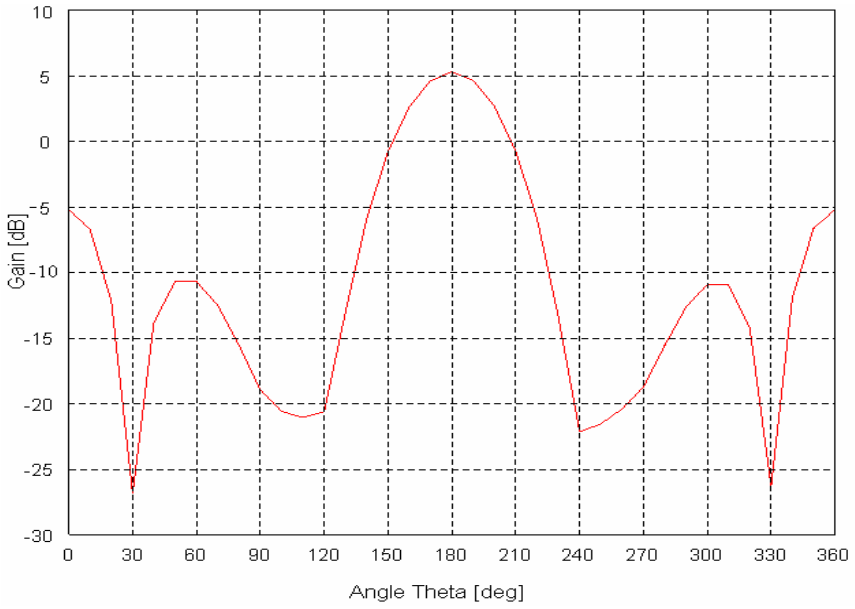

Figure 3.17: Gain characteristics of the simulated Shielded Butterfly antenna at 7GHz

From the plots shown in Figure 3.14 – 3.17, the characteristics of the simulated antenna can be sumarized as follows. It can be inferred from Figure 3.14 and 3.15 that the matching is not appropriate. Again, the simplified wire feed, which is used for the preliminary simulations, is mainly responsible for this mismatch. The original model presented in [11], makes use of a coaxial differential feed terminating at 50 Ohms each. The simplified wire feed used for the simulation purpose is not perfectly terminated at this impedance value. Further, the presence of the wire feed has a reactive influence, which is apparent from the impedance plot in Figure 3.16. The resistance plot also does not show any resonance as seen from Figure 3.17.

The gain of the antenna is around +5dB over the operating frequency. The gain characteristics at the center frequency of 7 GHz is shown in Figure 3.17. It can also be noticed that the simulated antenna has a good front to back ratio (FBR) of around 10 dB. This is mainly due to the use of the shield which helps in the reduction of the back radiation to a large extent apart from increasing the overall gain.

3.3.2 Realisation challenges in LTCC

A thorough analysis of the antenna with respect to the requirements is made based on which it is evident that the antenna can be implemented in the project's frequency range of interest. Nevertheless, the inclusion of the back shield will not allow the miniaturization of the antenna

beyond a certain limit, after which it will be practically challenging to realise it in LTCC. The main issue here is the shortcoming in the LTCC technology to model the metallic plates which form the back shield. The realisation of a continuous metallic plate is not possible in LTCC, which allows only grided planes to be realised instead. Another issue is concerned with the use of the via-holes for the fabrication of the back shield. These issues are of great concern as the most important element of this antenna is its back shield. Also, a direct differential feeding for the antenna at the 60GHz frequency range would be very demanding as the dimensions need to be downscaled accordingly. Further, precise fabrication of the feeding structure is also a complicated process, especially at mm-wave frequencies. The above mentioned limitations practically rule out the realisation of this antenna in LTCC technology.

3.4 Comparative Analysis

Subsequent to the deduction of the Shielded Butterfly antenna from the list of candidate antennas, due to the serious challenges for its realisation in LTCC, this section provides a comparative analysis between the Vivaldi and the Stacked Patch antennas. The analysis is carried out with respect to the main performance metrics. The Vivaldi as well as the Stacked Patch antenna can operate in a sound manner in the frequency range of interest (60 – 70 GHz) without much issue. The realisation in LTCC is also feasible as is evident from [8] and [13]. Further, the model in [13] also has an embedded air cavity.

Beamwidth: The Stacked Patch antennas provide a beam-width of around 90 degrees in both E and H planes [13]. The shape of the top patch decides the symmetry in beam-width between the E and H planes. A square patch usually gives a beam-width which is equal in both the planes. The Vivaldi antenna inherently, due to its end-fire operation provides a different beam-width between the E and H planes. This is due to the structure of the antenna which has an opening broader with respect to the E plane compared to the H plane making the E-plane beamwidth larger.

Radiation characteristics: From the publications related to the realisation of the Stacked Patch as well as the Vivaldi, it is observed that both these antennas have a positive gain throughout the entire operating bandwidth. The gain values obtained in the [8] and [13] are however less than the requirements of the project. Further as explained in Section 3.1.1, the characteristic of the Vivaldi antenna to radiate in both forward as well as the backward directions at lower frequencies of the operational bandwidth was a major factor which goes against its use as per the requirements of the project.

Miniaturization is possible for both these antennas as designs with dimensions less than 2 cm have been presented in [8] and [13] for the Vivaldi and the Stacked Patch antennas respectively. The dimensions of the Vivaldi are 14 x 8 mm and that of the Stacked Patch are 20 x 15 mm. A summary of the comparative analysis of the candidate antennas is presented in a tabular form below (Table 3.1).

Parameter	Vivaldi	Stacked Patch	Shielded Butterfly
Frequency band of operation	Wide to extremely wideband operations possible	Wideband operations possible	Wideband operations possible
Beamwidth	Inherently different in the E and H-planes	Wider beamwidth possible (~90-100^{o})	Wide beamwidth possible (~120^{o})
Gain	0 to +5dBi	0 to +5 dBi	+6 to +10 dBi
Size	Miniaturisation possible	Miniaturisation possible	Miniaturisation limited due to the shield
Differential feeding	Usage unknown	Few proposed design available	Feeding at 60 GHz would be complicated
LTCC issues	No unknown realisation complications	No unknown realisation complications	Realisation of the shield with the step pattern extremely complicated

Table 3.1: Summary of the comparative analysis of the candidate antennas

3.5 Selection of Final Candidate Antenna

The choice of the final antenna was made after a detailed investigation of the three candidate antennas with respect to their characteristics, with a special emphasis on the realisation process and the use of a differential feeding structure. The Stacked Patch antenna has features which are more attractive compared to that of the Vivaldi antenna. There is a lack of mainstream publications addressing the use of a differential feed for the Vivaldi antenna. The use of the differential feeding for the Stacked Patch antenna is also not very prevalent, but there are publications which present designs using differential feeding with broad bandwidth. These techniques can be used for the final/main antenna's design. The issue of nonlinear phase characteristics and the ringing in the time domain in the case of the Stacked Patch antenna are dispensed with. This is affirmed from the phase characteristics shown in Figure 3.12(a), which shows that the phase is fairly linear over the operating bandwidth. The ringing problem is also not severe enough to affect the performance (Figure 3.12(b)). The Stacked Patch antenna configuration can also achieve the required bandwidth. Besides

this, the antenna is well suited for use in a planar array arrangement. Hence, the Stacked Patch antenna is chosen as the final candidate antenna due to its inherent advantages over the other two antennas.

4

TESTED ANTENNA DESIGNS

This chapter discusses the Stacked Patch antenna configurations which were considered prior to the final antenna design. The numerical models of these configurations were also implemented using the EM solvers. Basically, two types of Stacked Patch antenna configurations were analysed and implemented. The study provided useful insights, which were incorporated into the final antenna's design. The geometrical description and the results which were obtained using these are presented in the remaining sections of this chapter.

4.1 Single Pin-Fed Stacked Patch Antenna with Air Cavity

The first Stacked Patch model implemented was with a single pin feed. The antenna configuration is derived from [13], which presents a similar structure operating in the 30GHz frequency range. The antenna was essentially implemented to study about the bandwidth and radiation characteristics which can be expected from a similar type of Stacked Patch, with the use of a differential feeding structure and dielectric substrates with high permittivity which is typical in LTCC technology.

4.1.1 Numerical Model of the Antenna Geometry

The antenna's geometry was rather simple with two patches, a single pin feed and an air cavity in the region between the two patches. The dielectric permittivity of the substrate was kept at 7.4 equal to that of the substrate which would be used for the fabrication process (DuPont's DP-943). The requirement of using a substrate with a higher dielectric permittivity in itself, presents a huge challenge with respect to the achievable bandwidth. A special emphasis was given to the bandwidth and the radiation characteristics. The inclusion of the air cavity helped in increasing the bandwidth of the antenna by 2-3GHz [13]. The side view of the antenna is provided in Figure 4.1. The numerical modeling of the structure was implemented using FEKO.

4.1.2 Optimization of the patches

The patches were optimised by using the optimization modules in OPTIFEKO. The initial dimensions of the patches were kept equal to half of the dielectric wavelength (λ_d=1.7mm). The final dimensions of the patches were fixed after using OPTIFEKO's optimization results and some theoretical fine tuning. The values of the patch dimensions (both length and width) were varied between 0.5mm to 1.1 mm. The final dimensions of the patches are presented in Table 4.1. The substrate heights were also optimized for maximum coupling between the two patches and also to reduce the unwanted surface currents which may be present due to the use of a high dielectric permittivity substrate. The guidelines given in [16] were used for the optimization process.

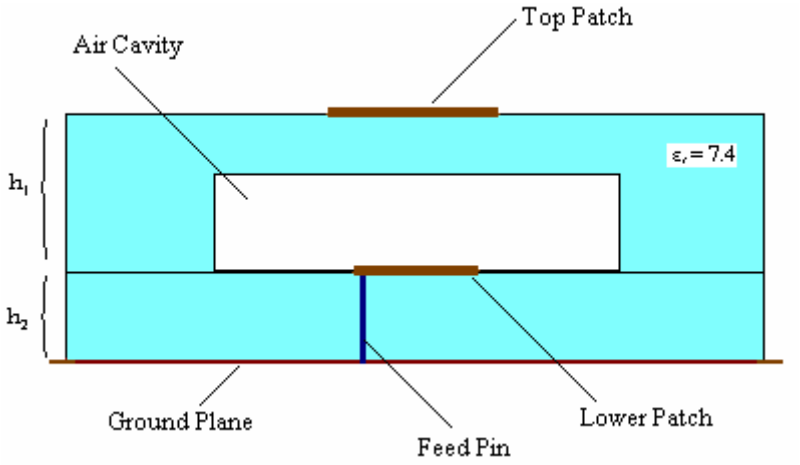

Figure 4.1: Side view of the Stacked Patch antenna with a single pin feed

The bandwidth, impedance and the radiation characteristics of the simulated antenna are presented in Figure 4.2, 4.3 and 4.4 respectively. It can be observed that the modelled antenna has an

impedance bandwidth of around 9.6 GHz (from 58.8 to 68.4 GHz). The main lobe gain is around 3 dBi. The "ideal" characteristic is due to the use of an infinite ground plane (*Green's function*) below the antenna structure. Finally, from the impedance plot, it can be seen that the imaginary part is inductive in the required frequency band (60-70GHz). This is mainly due to the inductive effect introduced by the feed pin. Also, similar to the preliminary design mentioned in Chapter 3, there was no mechanism to counter act this inductive effect. However, it can be seen that the value of the reactance is considerably low in the frequency band of interest.

Variable	Value in mm
Top Patch length	0.7
Top Patch width	0.75
Lower Patch length	0.9
Lower Patch width	0.7
h_1	0.520
h_2	0.208
Air cavity height	0.312
Substrate length	8
Substrate width	8

Table 4.1: Dimensions of the Pin-Fed Stacked Patch antenna

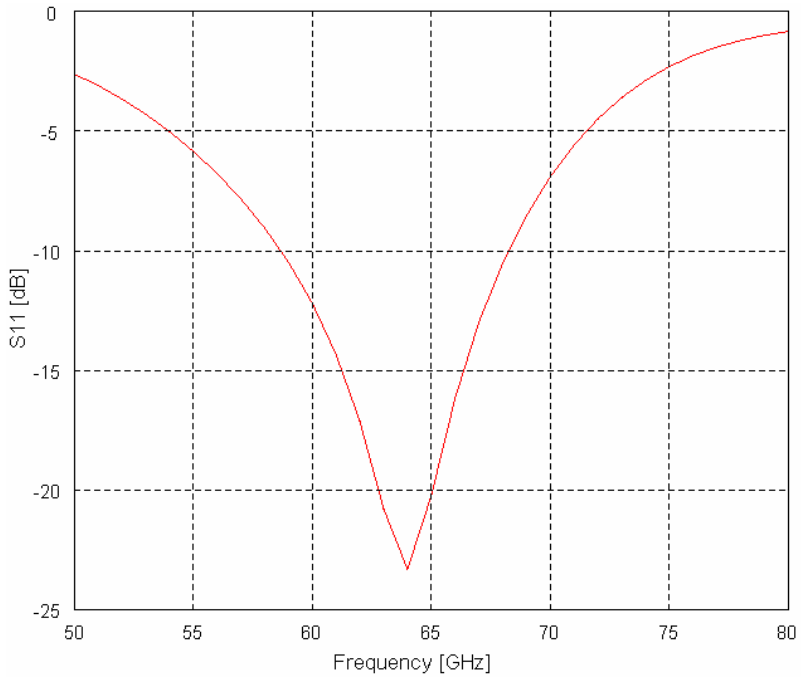

Figure 4.2: S_{11} characteristics of Stacked Patch antenna with a single pin feed

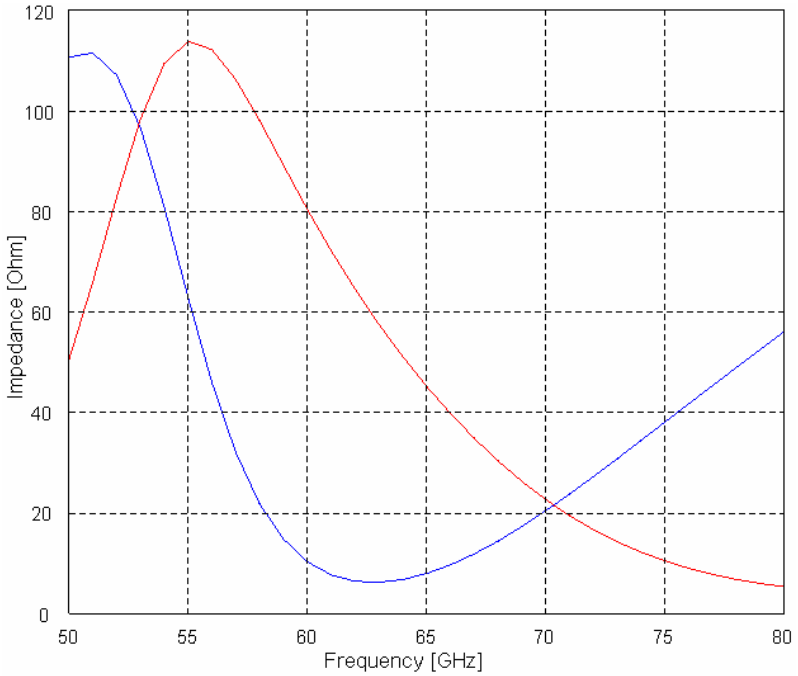

Figure 4.3: Impedance characteristics of the Stacked Patch antenna with a single pin feed

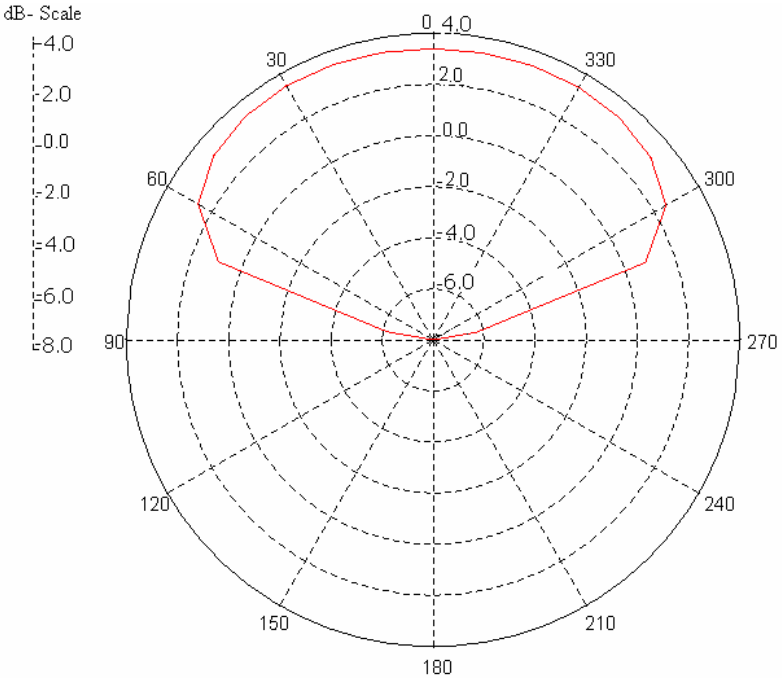

Figure 4.4: Radiation characteristics of the Stacked Patch antenna with a single pin feed

4.1.3 Summary of the results

The above plots show that the Stacked Patch antenna, modelled with a single pin feed, provided the necessary impedance, gain characteristics and bandwidth. The main shortcoming with the model presented with respect to the requirement was that it lacked a differential feeding structure, as it used a single pin feed.

4.2 Aperture Coupled Microstrip Stacked Patch Antenna

The design presented in [17], was considered as a possible candidate for implementing the differential feeding structure. The bandwidth requirement of the project is higher than that presented in [17]. The use of a substrate with a higher permittivity decreases the dielectric wavelength, which in turn down scales the dimensions of the components to a large extent. Apart from this, the antenna implemented in CST, was a Stacked Patch configuration compared to the single patch configuration proposed in the original model. The modelling and the subsequent results for this configuration, with the required modifications as mentioned, are presented next.

4.2.1 Numerical Model of the Antenna Geometry

The numerical model in CST is shown in Figure. 4.5. A balanced Microstrip feeding structure was used to feed the antenna model. Besides this, the antenna was an aperture coupled structure where the aperture slots coupled the energy to the patches above it. The slots were present in the intermediate ground plane of the structure.

4.2.2 Summary of results

The optimization process with respect to the patch dimensions and also the feeding structure dimensions did not yield any positive results. Hence, the dimensions of the configuration which at least had a "quotable" performance are given in Table 4.2. The main characteristics of the antenna obtained with these dimensions are shown in the Figure 4.6, 4.7 and 4.8.

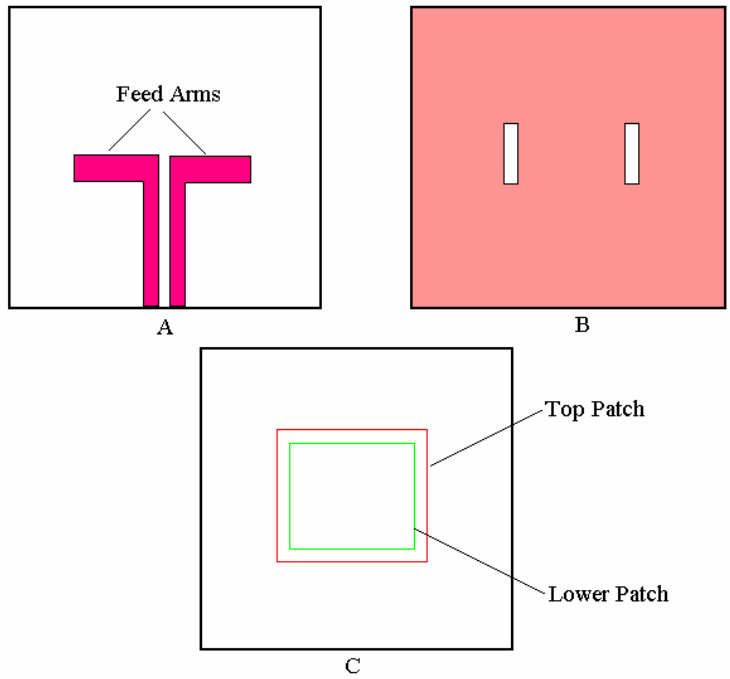

Figure 4.5: Layered view of the Microstrip Stacked Patch antenna with Aperture Coupling. A) Microstrip Feeding Structure, B) Ground Plane with radiating slots and C) Top view of the two patches used.

Variable	Value in mm
Feed arm width	0.25
Feed arm length	1.275
Feed separation	0.07
Stub length	0.42
Slot length	0.8
Slot width	0.2
Slot separation	1.3
Lower patch length	0.9
Lower patch width	1.45
Top patch length	0.9
Top patch width	1.65
Substrate length	8
Substrate width	8

Table 4.2: Dimensions of the Aperture Coupled Microstrip Stacked Patch antenna

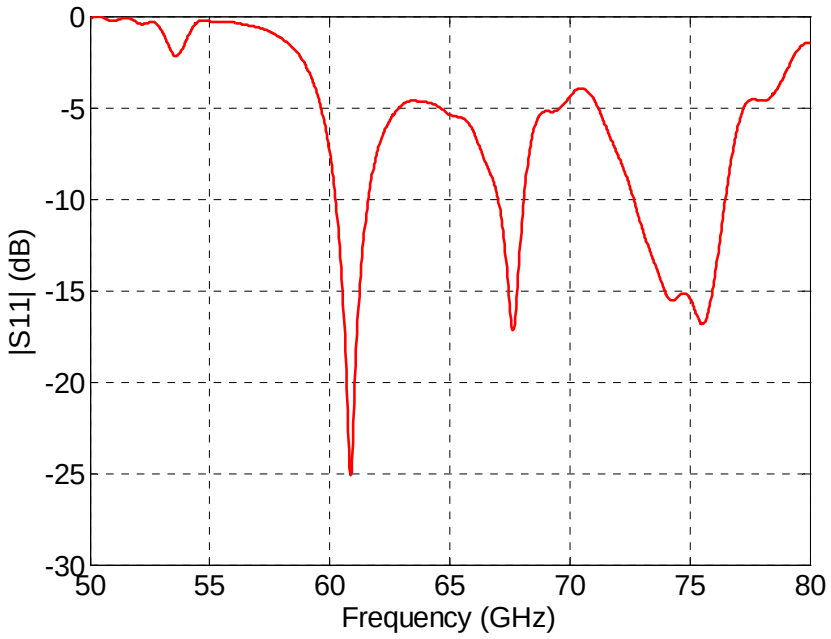

Figure 4.6: S_{11} characteristics of the Aperture Coupled Stacked Patch antenna

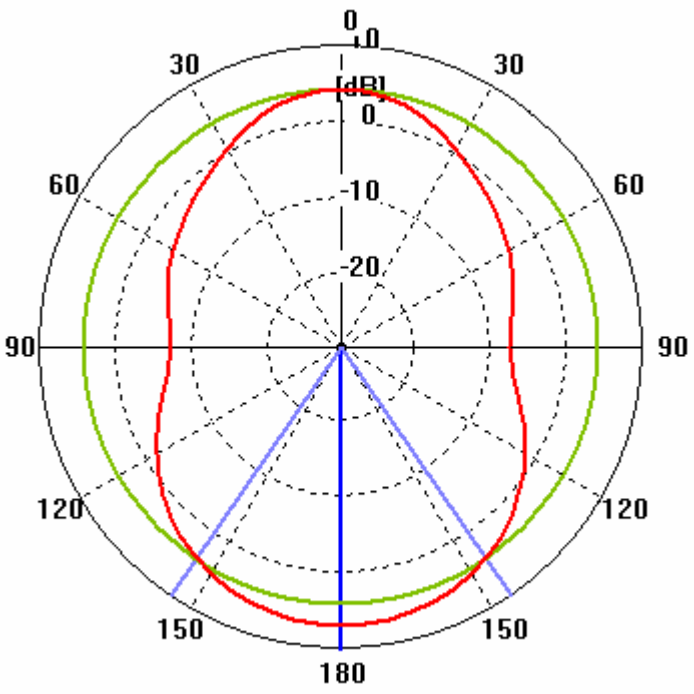

Figure 4.7: Radiation characteristics of the Aperture Coupled Stacked Patch antenna at 61 GHz

It can be inferred from the plots above that the antenna does not provide the required bandwidth of operation (~10GHz). Only a very narrowband of operation is achieved. This can be attributed to the use of the Microstrip feeding structure, which usually has a narrowband performance. The very high permittivity of the substrate (ε_r=7.4), also lowers the bandwidth possible, as the substrate permittivity has an inverse relation with the achievable bandwidth. Further, the radiation pattern is also not optimal. The main reason is that patch dimensions are just enough to cover both the slots and so independent radiations from the slots are also possible which deters the radiation characteristics. It can also be seen that the backward radiation is high compared to that of the forward radiation. The presence of a reflector patch below the Microstrip feeding acts as a radiating patch for the feeding structure. The Microstrip lines resemble a dipole which might increase the radiation further in the backward direction. The entire geometry with an intermediate ground plane, did not serve the requirement well. However, the configuration does not have any problems with respect to the realisation in LTCC. These results meant that the configuration had to be changed significantly to provide acceptable performance. Hence, this antenna configuration was dispensed with.

5

APERTURE COUPLED STACKED PATCH ANTENNA with DIFFERENTIAL FEEDING

This chapter presents the **novel** design and optimization of a differentially fed Aperture Coupled Stacked Patch antenna configuration. The inspirations for the final antenna design are taken from [18] and [19]. A differential feeding structure which could be used for the Stacked Patch antenna is presented in [19]. Differential feeding configuration as presented in [20], was also considered, but neglected as the size of the proximity feed structure will be too small to be manufactured within the tolerance limits for operations in the mm-wave frequencies.

5.1 Overview of the Design

The antenna is essentially an aperture coupled stacked patch antenna using differential feeding. The antenna has a coupling aperture, which is differentially fed in substrates with high dielectric permittivity achieving a wide bandwidth of operation. These aspects account for the **novelty** of the design. An H-shaped coupling aperture is used in place of the conventional rectangular slot aperture for achieving higher bandwidths. The antenna's layered and side views are shown in Figure 5.1 and 5.2 respectively. The aperture slot and the feed points are shown in Figure 5.3.

Air Cavity

Although an air cavity helps in achieving higher bandwidths as shown in Section 4.1.2, it is avoided in the design due to the complications with respect to its realisation in LTCC. The air cavity can be realised only by means of a laser drill, which is time consuming as well as expensive comparatively. Thus the design presented apart from achieving the necessary performance is **simple** and **easily realizable** in LTCC technology.

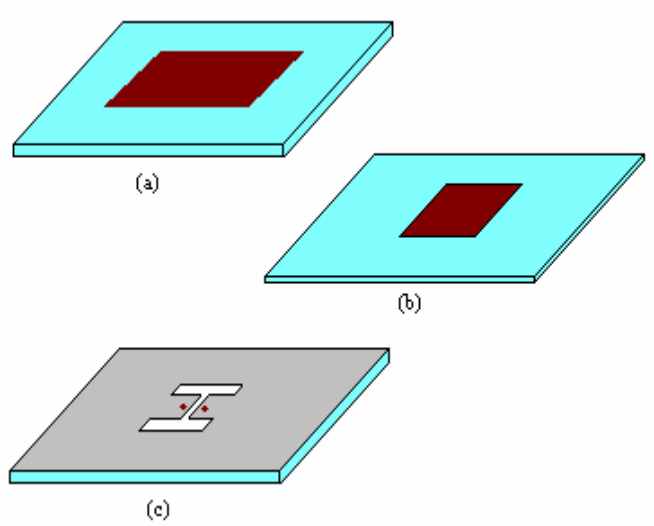

Figure 5.1: Layered view of the antenna geometry, (a) - top patch, (b) - lower patch, (c) - Aperture slot and Intermediate ground plane

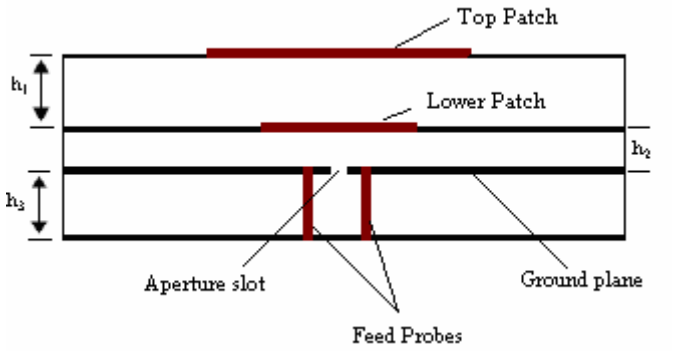

Figure 5.2: Side view of the antenna geometry (ε_r=7.4)

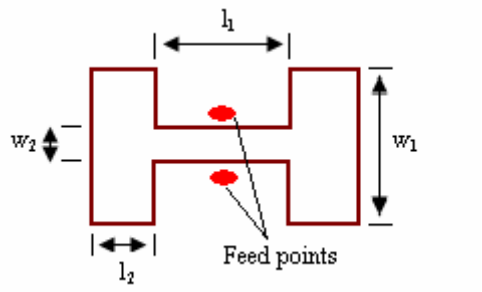

Figure 5.3: H-shaped aperture and differential feeding points

The antenna's feeding excites the aperture slot, which in turn couples the energy to the patches above it. The stacked patch configuration chosen in place of the usual single patch design achieves higher bandwidth. The intermediate ground plane which contains the aperture slot helps in reducing the backward radiation, thereby increasing the front-to-back ratio (FBR). This is an important characteristic, as the proposed antenna is to be integrated with a MMIC. A lower back radiation ensures less interference with the MMIC and also improves the radiation characteristics.

5.1.1 Differential Feeding Structure

The feeding structure used is shown in Figure 5.2. The use of a differential output from an MMIC to feed the antenna requires the feeding to be differential as well. In order to account for this condition, a feeding structure with two parallel probes as shown in Figure 5.2 is used in the design. This configuration also serves the requirements as the differential output from the MMIC can be directly placed in contact with these probes. The feeding probes are located symmetrically on either side of the center slot as shown in Figure 5.3. This type of feeding has been proven to provide good radiation patterns, apart from offering a wide bandwidth of operation [18]. These probes excite the aperture cavity, from where the energy gets coupled to the patches above.

5.1.2 H-Shaped Aperture Slot

The H-shaped aperture slot is chosen instead of the normal rectangular slot for achieving higher coupling and lower back radiations. Aperture coupled Stacked Patch antennas with rectangular slots were first proposed by Pozar [21]. Stacked patch antennas with aperture coupling have bandwidths between 7-60%, presented in various research works. The aperture slot used in the antenna design is shown in Figure 5.3.

5.2 Choice of the EM solver

The choice of the EM solver is made based on the requirement and the size of the structure. This study involves the analysis of the reflection coefficient and the radiation pattern of the antenna. Further, the antenna operates in the mm-wave frequencies which automatically decreases the size of the antenna to few tens of millimeters (requirement < less than 2 cm). Therefore, it can be inferred that the size of the antenna structure to be simulated will be only 5-6 times the dielectric wavelength (λ_d=1.7mm). This means that the analysis can be made more accurate by using volumetric

discretization techniques instead of the surface discretization techniques (as used in FEKO). CST, which uses the volumetric discretization technique, is chosen for the analysis. It is a time domain solver based on the Finite Integral Technique [27]. The use of a time domain solver helps in obtaining the required characteristics for all frequencies over the entire operating bandwidth. This is due to the fact that the solver essentially excites the structure using very short time domain pulses, typically having periods in terms of nanoseconds. It can be seen from the antenna configuration shown next, that the structure is not entirely homogeneous. CST is also better suited (than for example FEKO) to simulate and study structures with in-homogeneity. Hence, CST is chosen as the numerical solver for the simulation and analysis purposes.

5.3 Optimization Procedure

The optimization procedure was carried out to accomplish the bandwidth and the radiation characteristic requirements of the antenna. Each of the parameters as given in Table 5.1, are separately optimised for the projects requirements in terms of impedance bandwidth and radiation characteristics. The following sections elucidate the optimization procedures carried out for each of the parameters in Table 5.1, the results obtained and their final dimensions. A mesh size equal to $\lambda_d/35$ is maintained for the optimization process. The numerical approximation implemented for the optimization and the subsequent analysis is presented in Appendix B.

Order of optimization

The optimization process was undertaken in the following order. The initial dimensions of all the components in the antenna's geometry were fixed according to considerations as will be explained in the subsequent sections. As the first step, with the initial dimensions of the feed pins, the optimization test runs for the feed pin dimensions and separation were undertaken to get the maximum excitation. The dimensions of the patches were then optimised to get the resonances in the required frequency band of operation. This was followed by the optimization of the aperture dimensions to test its influence on the characteristics. These steps helped in analysing the mutual coupling behaviour between the patches and the aperture slot, a factor which is very important for the bandwidth. The substrate heights were also optimized. When the required bandwidth of operation (≥10GHz) and the radiation characteristics (positive gain and FBR≥15dB) were obtained, the influence of the grided plane on the performance of the antenna was studied. The results of the grided plane's influence are presented towards the end of this chapter. The optimization process

was based on the guidelines given in [16], 18], [19] and [20], where similar optimization strategies are followed for the stacked patch antennas presented in them.

Parameters
Length and width of Top Patch
Length and width of Lower Patch
Aperture Dimensions
Substrate thickness
Diameter of the feed pins
Separation between the feed pins

Table 5.1: Parameters for optimization

5.3.1 Optimization of the Patches

The parametric study was carried out with respect to the length and width of both upper and lower patches. The numerical model with the structure defined in Section 5.1, simulated in CST was used for the parametric study. The initial values of the length and width of both the patches were kept equal to half of the dielectric wavelength (λ_d=1.7mm) at 0.85mm.

The width of the lower patch (LW) was varied from 0.5mm to 1.2 mm. The results obtained for this optimization are shown in Figure 5.4. It can be seen that there are two resonances for a values of 0.6mm and 0.7mm in the frequency range of interest (60-70GHz). Therefore a value of 0.6mm was fixed for the width of the lower patch (LW). A similar procedure was carried out for the width of the top patch (TW) by varying it between 0.5 – 1.2 mm. The results are shown in Figure 5.5.

By fixing the width of both upper and lower patches equal to 0.6mm, the optimization procedure was continued further for the length of lower patch (LL), by varying it between 0.7 to 1.4mm. The results for this are shown in Figure 5.6. The values of LL corresponding to 0.8mm and 0.9mm were used for the optimization of the top patch length (TL). The length of the top patch (TL) was varied between 0.85 and 1.85mm. Only the plot for the optimization of length of the top patch, with LL having a value of 0.8mm is presented in Figure 5.7 as the latter value of LL did not satisfy the requirement.

It can be inferred from the plots that with the variation in the width of the lower as well as the top patch there is a noticeable change in the frequency at which the resonances occur. This is primarily due to the fact that the patch dimensions are scaled in terms of λ_d, and hence a change in the length corresponds to a different λ_d, which in turn translates into a different frequency value. With the

change in the value of the length of the lower as well as the top patch there is a variation in the steepness of the curve. This demonstrates that with the change in the values of the length the amount coupling at the corresponding resonances change as well. This is due to the fact that with the increase or decrease in the length of the patches, the effective impedance due to the patches also increases or decreases correspondingly.

The required bandwidth was achieved with the following sets of dimensions; 1) TL = 1.75mm, LL=0.8mm, TW=0.6mm LW=0.6mm and 2) TL=1.85mm, LL=0.8mm, TW=0.6mm, LW=0.6mm. However, the first set of dimensions was chosen as the bandwidth achieved is 0.6GHz greater than the other set.

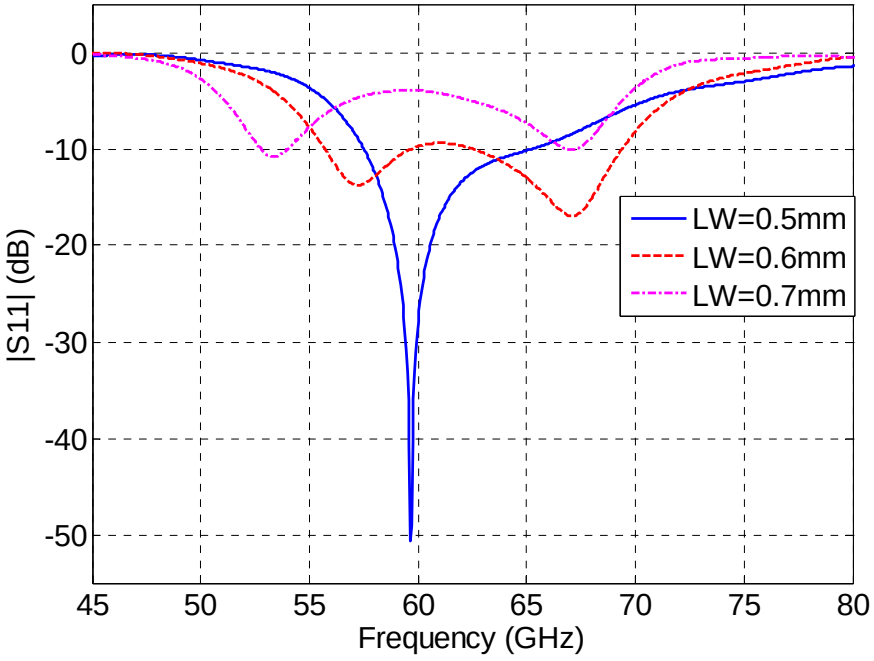

Figure 5.4: Optimization of the width of the lower patch (LW)

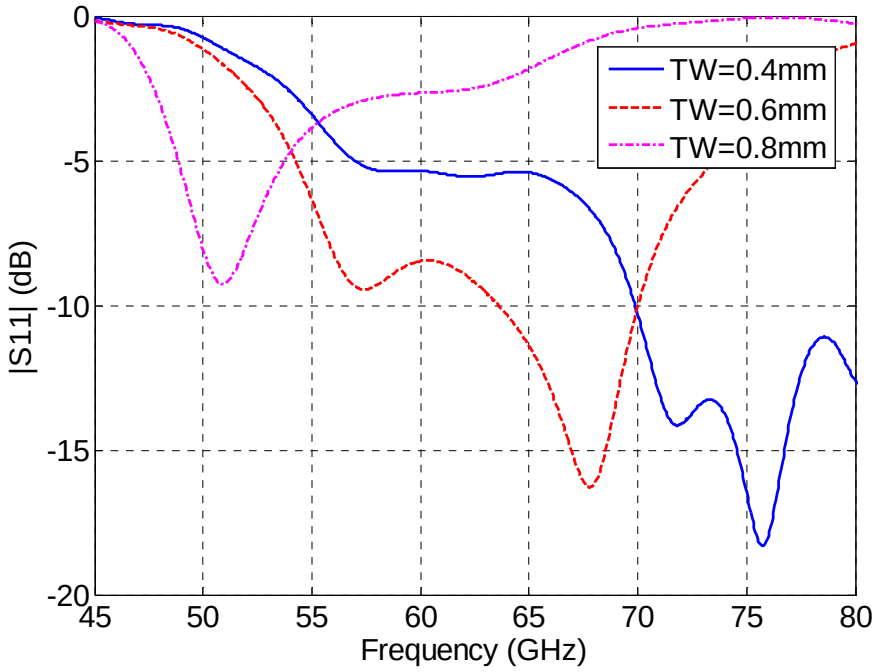

Figure 5.5: Optimization of the width of the top patch (TW)

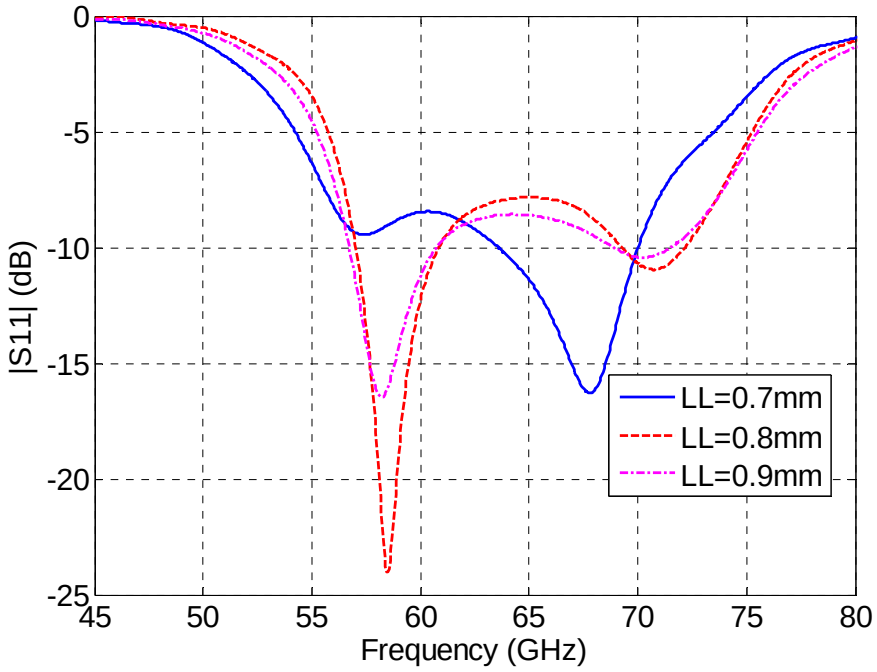

Figure 5.6: Optimization of the length of the lower patch (LL)

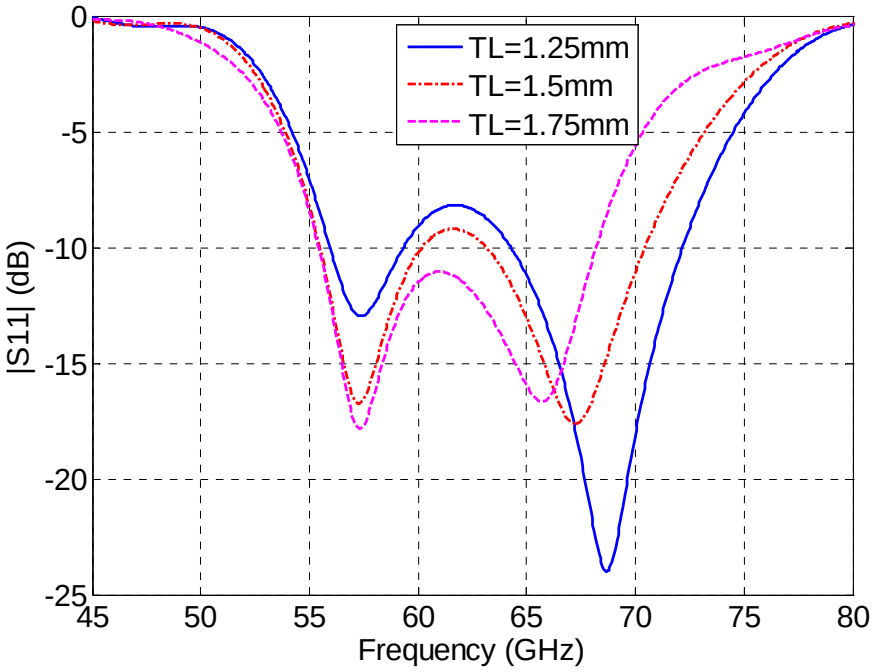

Figure 5.7: Optimization of the length of the top patch (TL)

5.3.2 Aperture Dimensions

The dimensions of the H-shaped aperture can be described by means of four parameters viz. l_1, l_2, w_1 and w_2 (Figure 5.3). Compared to the conventional rectangular slots, which usually has one resonance, the use of an H-shaped slot helps in attaining two or more resonances. The resonances are dependent on the length of the center arm and the side arms of the H-slot. This is due to the fact that all the dimensions are in terms of the dielectric wavelength (λ_d). The resonant frequencies depend on the dielectric wavelength through the well known relation $f_c=c/\lambda_d$, where f_c is the resonant frequency and c being the velocity of light ($3x10^8$m/s)

In the context of designing the aperture for the antenna, it becomes important to understand the effect of each these parameters on the resonant characteristics of the antenna. An optimization procedure similar to the one presented in [19] was followed, with the required downscaling of the dimensions with respect to the mm-wave frequencies and the high dielectric permittivity of the substrate. The process involved the variation of the four parameters (l_1, l_2, w_1 and w_2), in steps between boundary values. The effect of the variations on the impedance and the S_{11} characteristics are studied. The final dimensions were fixed based on this study.

The initial dimensions of the parameters are set with guidelines given in [19]. The initial values in terms of λ_d for the four parameters are as follows, l_1=0.15 λ_d, l_2 =0.06 λ_d, w1 =0.09 λ_d and w_2 =0.03 λ_d.

Figure 5.8 shows the variation of the reflection co-efficient (S_{11}) with the corresponding variation of l_1. The test run was conducted by varying the value of l_1 between 0.2mm to 0.3mm, with a step increment of 0.01mm. It was observed that at lower values of l_1, the first resonance was steeper compared to the second and an opposite behaviour at values of l_1 greater than 0.26mm. In order to keep both the resonances "balanced", a trade-off value of 0.275mm was chosen for the final model.

The effects of l_2, w_1 and w_2 were also studied and were found to be similar to that of l_1 with the first resonance stronger than the second at lower values and the vice versa as the values increase. The value of l_2 was varied between 0.07-0.13mm, w_1 between 0.1-0.17mm and w_2 between 0.025-0.065mm. The final dimensions of the aperture, which were used for the subsequent modelling of the antenna are as follows; l_1=0.275mm, l_2=0.15mm, w_1=0.09mm and w_2=0.045mm. The plots for the optimization of l_2, w_1 and w_2 are shown in Figure 5.9-5.11 respectively.

It can hence be concluded from this optimization step that the dimensions of the H-shaped aperture primarily influence the amount of coupling. The dimensions do not influence the resonance frequencies. The behaviour is completely physical as the H-shaped aperture slot is primarily introduced into the configuration for better coupling and naturally should not influence any other characteristic drastically.

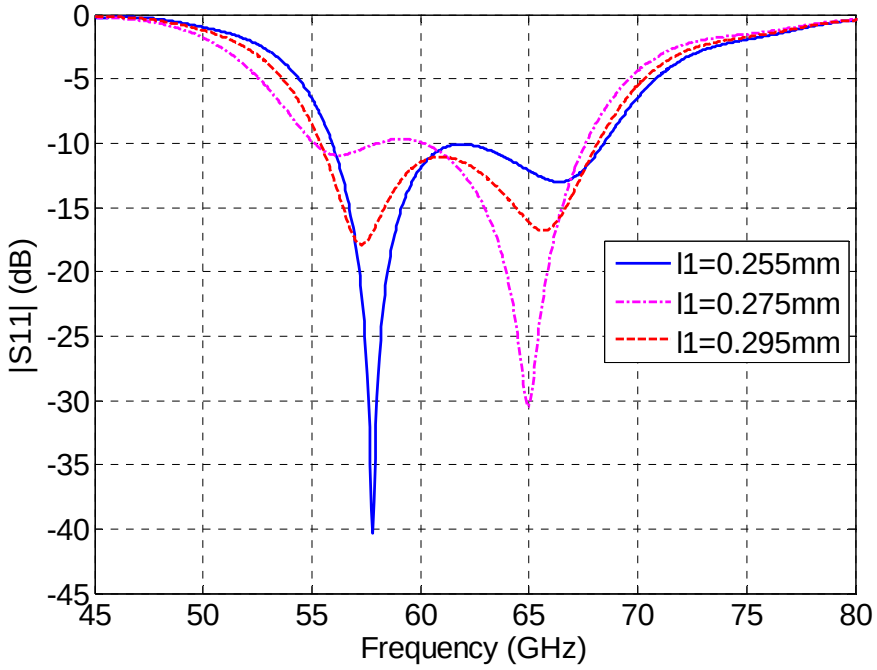

Figure 5.8: Optimization of l_1 (center arm length of the aperture)

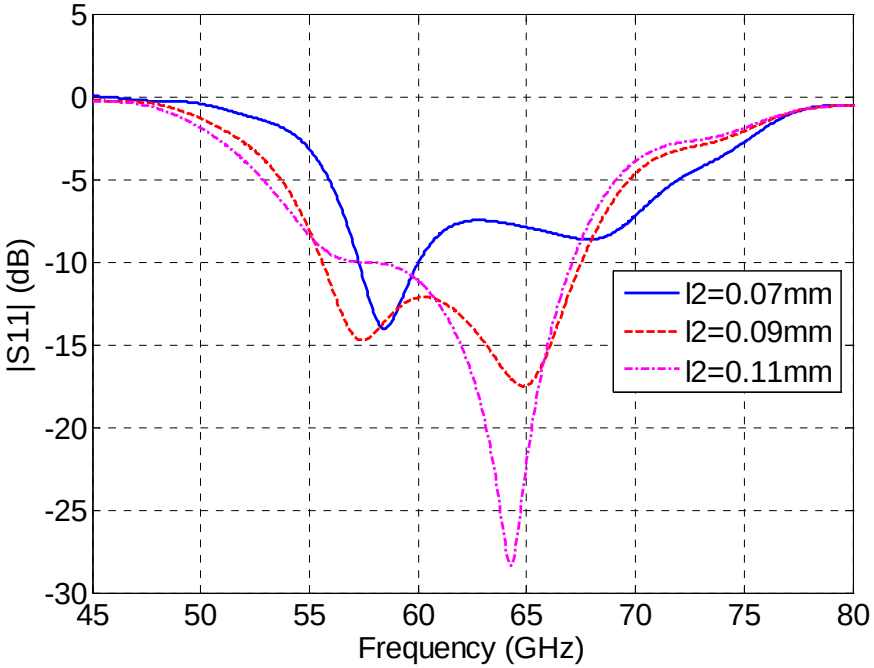

Figure 5.9: Optimization of l_2 (side arm width of the aperture)

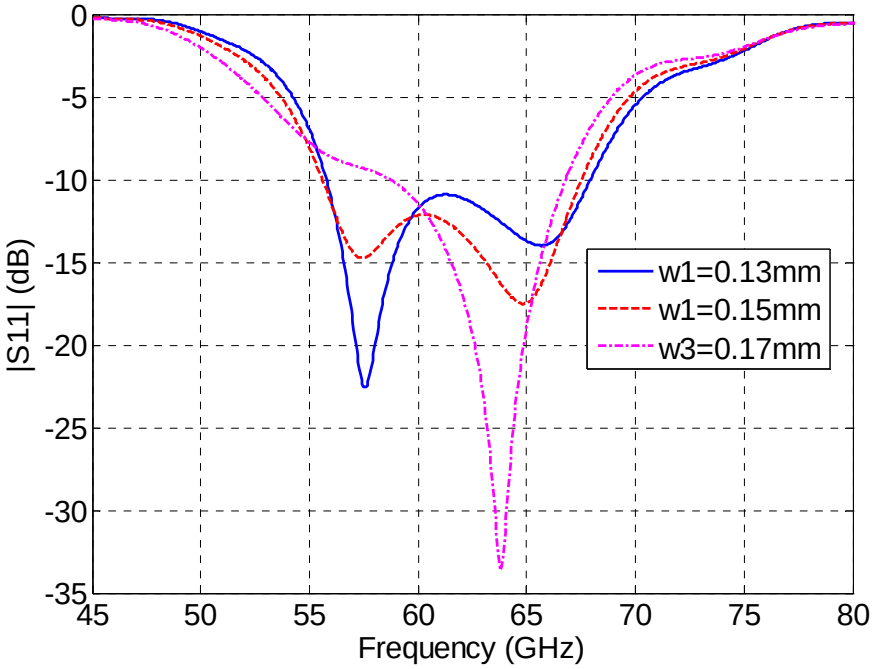

Figure 5.10: Optimization of w_1 (side arm length of the aperture)

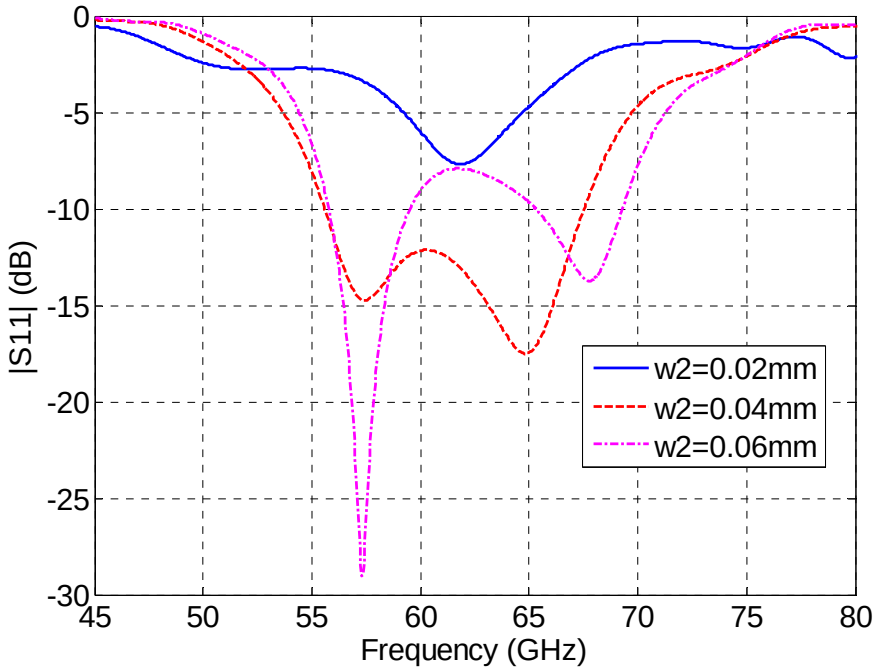

Figure 5.11: Optimization of w_2 (center arm width of the aperture)

5.3.3 Feed Pin Dimensions

The dimensions of the feed pin play an important role in the impedance matching. The antenna designed should have a differential feeding structure as per the requirements of the project. The differential feeding structure is implemented through the use of two pin feeds (probes), which run parallel to each other on either side of the center arm of the H-shaped aperture slot. The initial dimensions of the diameter of the pins as well as the separation between the two pins are set using the commercially available software AppCAD. The dimensions should be set to match to a reference impedance of 100Ohms. The diameter of the feed pins and the separation between them determine the amount of excitation in the slot. An increase in the pins diameter with the same separation increases the amplitude of excitation. The converse is also true if the diameters are decreased for the same separation. In either case it results in an impedance mismatch. In the optimization process a diameter of 70µm for the feed pins and a separation of 0.145 mm between them provided the necessary matching. A further study on the effect of the variation of the diameter of the feed pins and separation between them showed that the required characteristics can be achieved till an upper limit value of 90µm for the pin diameter and 0.165mm for the separation between them. Above these dimensions the characteristics are not maintained.

5.3.4 Substrate Thickness

The achievable bandwidth is also influenced by the substrate thickness. The height of the substrate could not be increased or decreased arbitrarily and can only be done in steps of layers. The thickness of a single layer is around 104μm. This was one of the constraints imposed on the design due to the LTCC fabrication. During the optimization process, it was found that an increase in h_1 (height between the two patches); apart from increasing the surface waves, did not result in a higher impedance bandwidth. This can be attributed to high dielectric permittivity (ε_r=7.4) of the substrate used. But, a very thin substrate has to be avoided as it would not only complicate the manufacturing process in LTCC [6], but also jeopardize the tensile strength of the antenna. A plot showing the effect of the substrate height between the two patches on the S_{11} characteristics is shown in Figure 5.12. A compromise between the two conditions resulted in the final dimensions with h_1=0.208mm (2 layers), h_2=0.104mm (1 layer) and h_3=0.208mm (2 layers). The bandwidth requirement was satisfied completely with these values and the unfavourable characteristics induced by the increase in the dielectric layers are thus excluded.

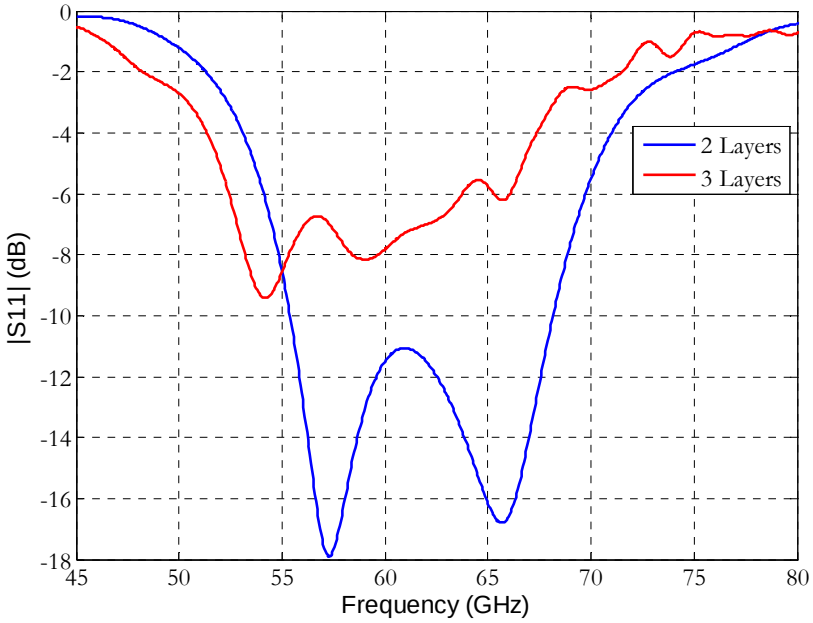

Figure 5.12: Influence of the substrate height on the S_{11} characteristics

5.3.5 Ground Plane and Substrate size

The gain pattern of the antenna also depends on the size of the intermediate ground plane. A bigger ground plane increases the Front-to-Back Ratio (FBR). In order to have a bigger ground plane the substrate size should be increased as well. The length and width of the ground plane are kept at 10mm and 8mm respectively. These values provide an FBR greater than 10dB. The substrate size is kept bigger than the ground plane as it will helpful during the fabrication process in LTCC, where the ratio of metallised to non-metallised area should be less than 50% of the total area. A final value of 10.25mm and 8.25mm are kept for the length and width of the substrate.

5.4 Final Antenna Dimensions

The antenna's final dimensions are as given in Table 5.2. The patches are kept rectangular. A square patch is not preferred as it might result in higher levels of cross polarization.

The gain characteristics and S_{11} for the antenna with the dimensions as given in Table 5.2 are presented in Figure 5.13, 5.14 and 5.15 respectively. It can be inferred from Figure 5.15, that the antenna has an impedance bandwidth of 13.5 GHz (55.2-68.7 GHz). This corresponds to a fractional bandwidth of 21.5%. A Smith chart representation of the impedance characteristics is shown in Figure 5.16. The antenna also has a good front-to-back ratio of around 12.2 dB (Figure 5.13-14). The main lobe amplitude is around 4 to 5dBi.

A plot of the forward as well as the backward direction gain at different frequencies of the operational bandwidth is provided in Figure 5.17. This implies that the antenna can be used with a MMIC at its rear without causing any interference to it over the entire operational bandwidth.

Variable	Value in mm
TL	1.75
TW	0.6
PL	0.8
PW	0.6
h_1	0.208
h_2	0.104
h_3	0.208
l_1	0.275
w_1	0.15
l_2	0.09
w_2	0.04
Feed port cylinder diameter	0.07
Substrate length	10.25
Substrate width	8.25
Ground plane length	10
Ground plane width	8

Table 5.2: Final Dimensions of the Aperture Coupled Stacked Patch antenna with differential feeding

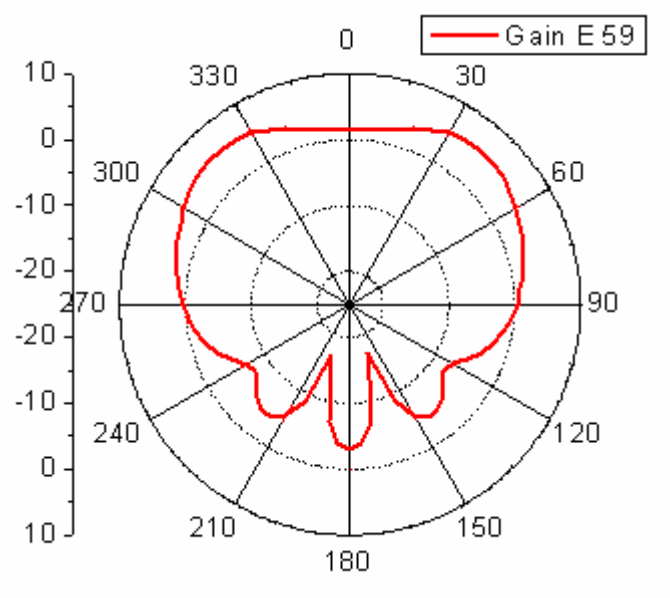

(a) E-Plane

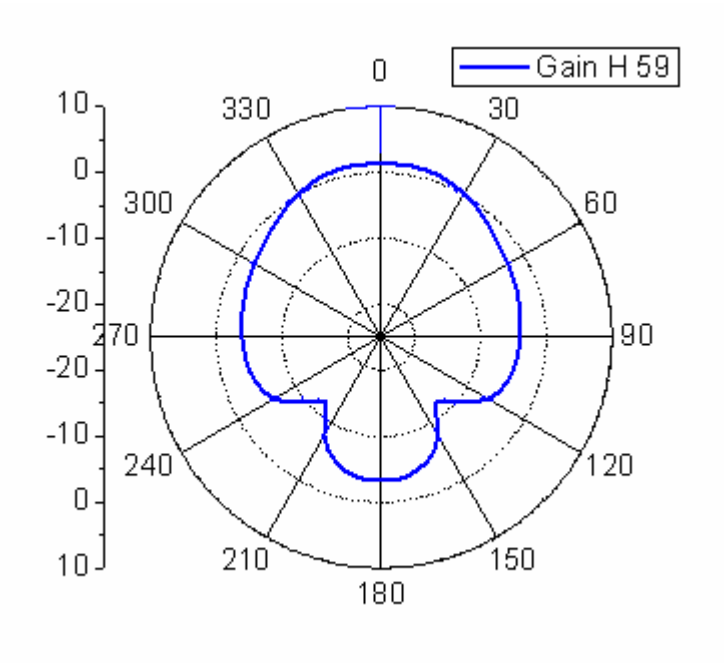

(b) H-Plane

Figure 5.13: Gain characteristics of the Antenna at 59 GHz.

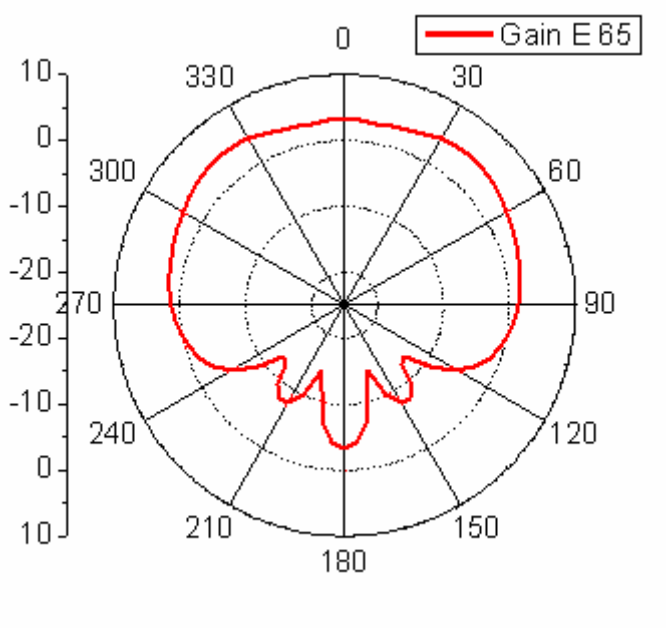

(c) E-Plane

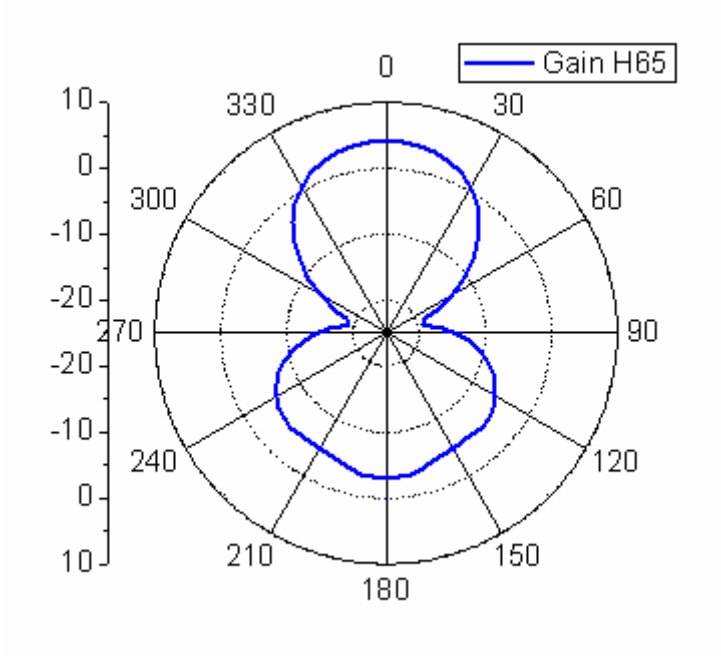

(d) H-Plane

Figure 5.14: Gain characteristics of the Antenna at 65 GHz.

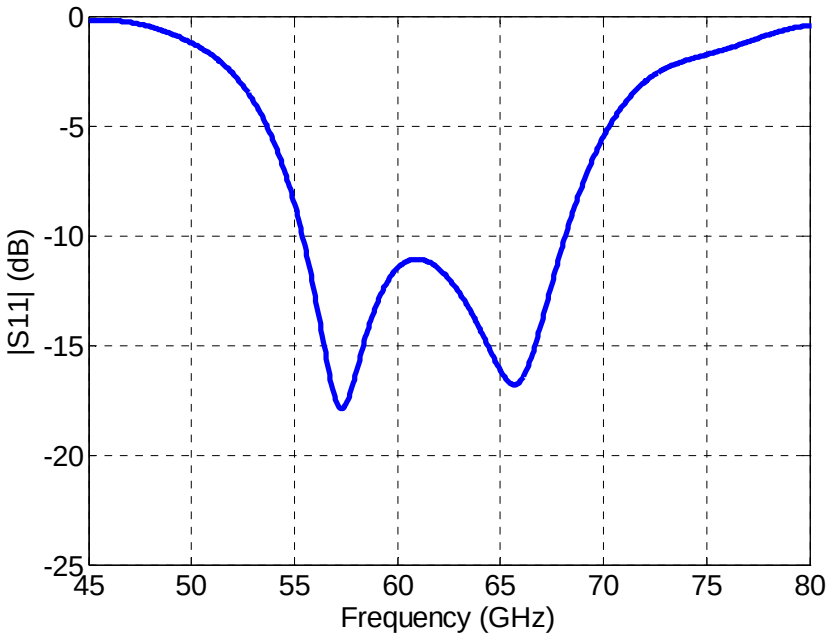

Figure 5.15: S_{11} characteristics of the antenna

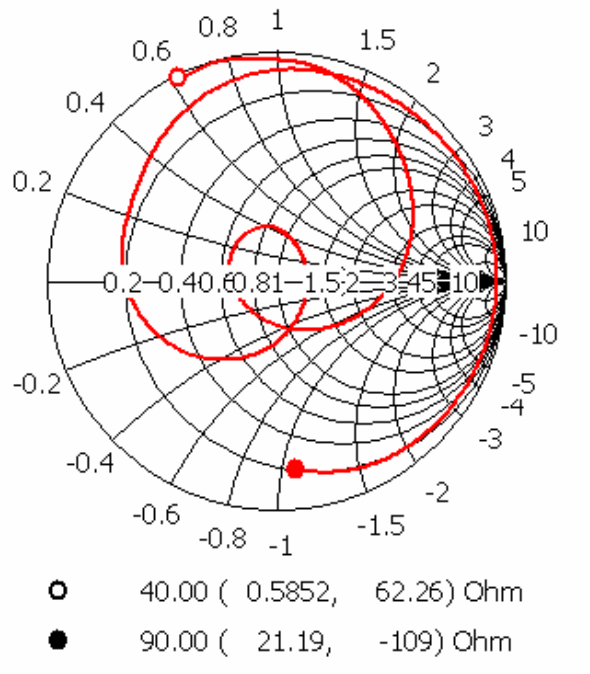

Figure 5.16: S-parameter Smith Chart of the antenna

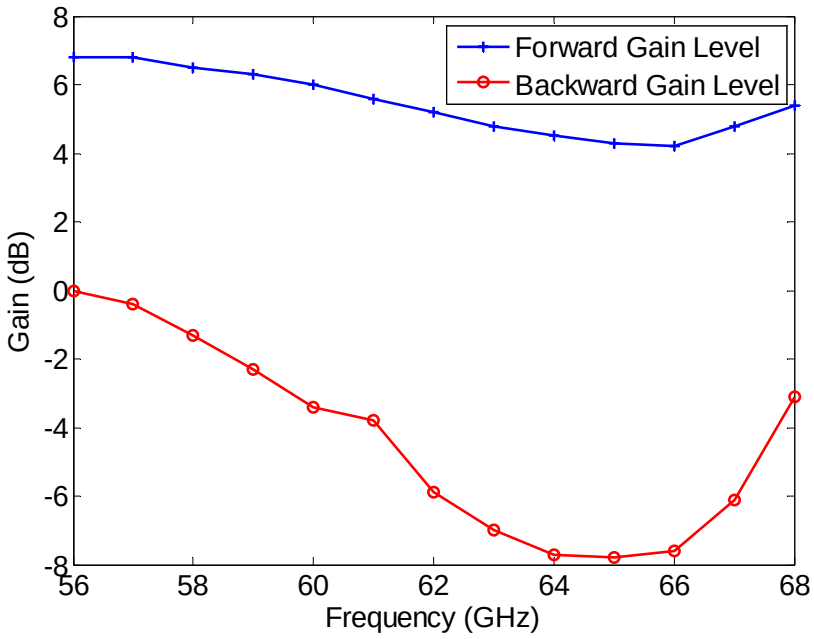

Figure 5.17: Forward and Backward Gain Vs Frequency

5.4.1 Discussion on the antenna gain and bandwidth characteristics

Bandwidth: The project requires an operational bandwidth of at least 10GHz in order to achieve higher resolutions. The bandwidth plot (S_{11}) of the antenna shows that the bandwidth of nearly 13.5GHz, which is obtained from 55.2 to 68.7GHz. However, this does not cover 60-70GHz band completely. Although the antenna falls short by around 1GHz of the 60-70GHz frequency range, it still has a bandwidth higher than that required in the project and hence can help in achieving higher resolutions. Fine tuning measures undertaken to shift the bandwidth in order the cover the whole bandwidth during the optimization process were not very successful.

Radiation characteristics: From the plot shown in Figure 5.17, it is evident that there is a good positive gain value (≥3dB) over the operational bandwidth along with a good front-to-back ratio (maximum 12.4dB). However, it can be noticed that the gain decreases with higher frequencies, with a maximum difference of around 3dB between the extremities in the gain values. This aspect can be attributed to the fact that a larger emphasis was kept on the bandwidth requirement compared to the radiation characteristics. The beamwidth of the antenna also increases slightly (5-10 degrees) with frequency. This behaviour will naturally, in-turn reduce the main lobe gain level. Nevertheless, the

radiation characteristics obtained satisfy the respective requirements of the project. Optimization of the configuration for "better" radiation characteristics may result in enhanced performance.

Efficiency: The total efficiency of the antenna as obtained from the numerical simulations varies between 0.91 and 0.98. These values reiterate the antenna's radiation effectiveness.

5.5 Issue of Grided Plane in LTCC

The antenna modelled with the configuration and dimensions as mentioned in the previous sections of this chapter is within the manufacturing limits. This makes it entirely realizable in the LTCC technology. However, in LTCC, the realisation of a continuous ground plane is not possible and only a grided plane is realizable. Nevertheless, this will not degrade the performance of the antenna extremely. This is clear from the short analysis which was carried out using a continuous intermediate ground plane and a grided plane. The length and width of the grid slots are kept equal to $\lambda_d/8$, which in this case is equal to 1.7/8mm≈0.22mm (λ_d =1.7mm). The value is chosen to keep the grid slots as large as possible to take into effect the maximum change in the characteristics due to the use of a grided plane. The usual size of the grid slots in the fabrication process is around λ_d /12 to λ_d /8. Hence, the approximated dimensions of the grid slots are well within the practical grid slot values of the LTCC process. The performance comparison was made between the two cases with respect to the main characteristics. The bandwidth characteristics for these two cases are shown in Figure 5.18. It is evident that the grided plane does not have a drastic influence on the characteristics of the antenna modelled. The radiation characteristics are also maintained without any major deviations. Hence the final dimensions as given in Section 5.4 are maintained as such for the realisation process. A layered view of the simulated grided ground plane is presented in the Figure 5.19.

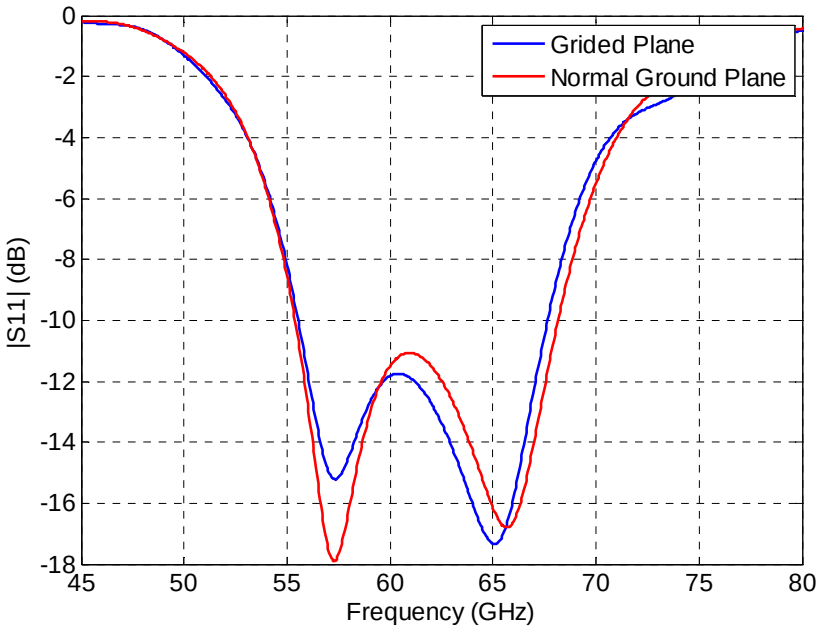

Figure 5.18: Influence of the grided plane

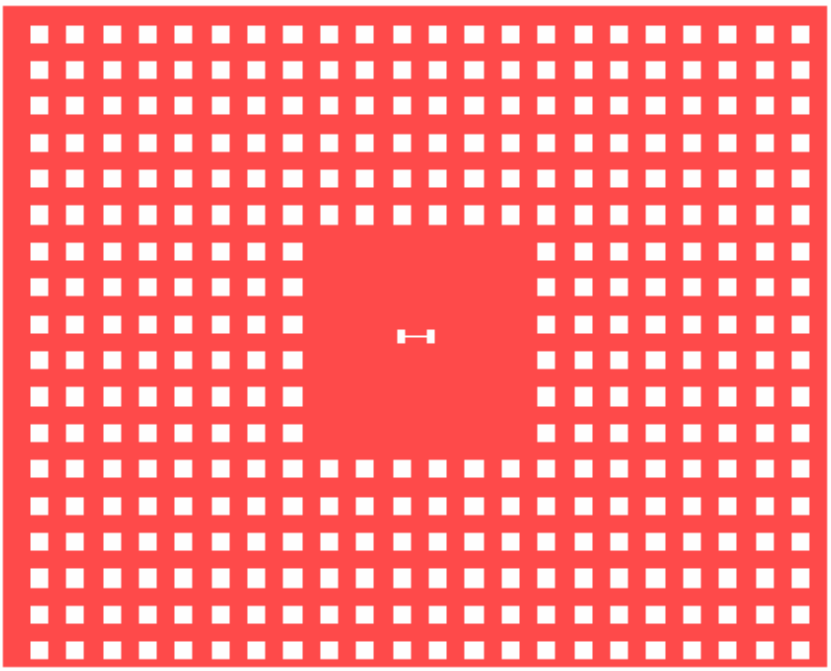

Figure 5.19: Layered view of the grided plane

5.6 Sensitivity of the characteristics Vs fabrication tolerances

In this section the sensitivity of the antenna characteristics on the fabrication tolerances is presented. The extent by which the characteristics vary with the deviations in the dimension values of the different components is elucidated.

Metal patches

Both the lower patch (length-0.8mm, width-0.6mm) and top patch (length-1.75mm, width-0.6mm) with their respective dimensions can be manufactured precisely. Also a very slight difference in terms of microns will not have a significant influence on the bandwidth characteristics. Hence, the sensitivity is not tested explicitly with respect to the patch dimensions.

Aperture dimensions

The dimensions of the aperture are within the tolerance limits as explained in the previous sections. However, since the values of the center arm width (w_2) and the side arm width (l_2) are less than 100 microns, the deviations with respect to these parameters are tested. Figures5.20 and 5.21 show the variation of the S_{11} characteristics with the deviation in the values of l_2 and w_2 respectively. It can be seen that the characteristics is maintained till a value of 0.1mm for l_2 and 0.45mm for w_2. It can also be noticed that the variation in the value of w_2 has a greater effect on the characteristics compared to that of l_2. Even for a change of 0.01mm for w_2, the variation in the S_{11} is quite significant. Hence, the fabrication tolerance with respect to w_2 should be of higher precision comparatively. The dimensions of the aperture slot do not have a significant impact on the radiation characteristics.

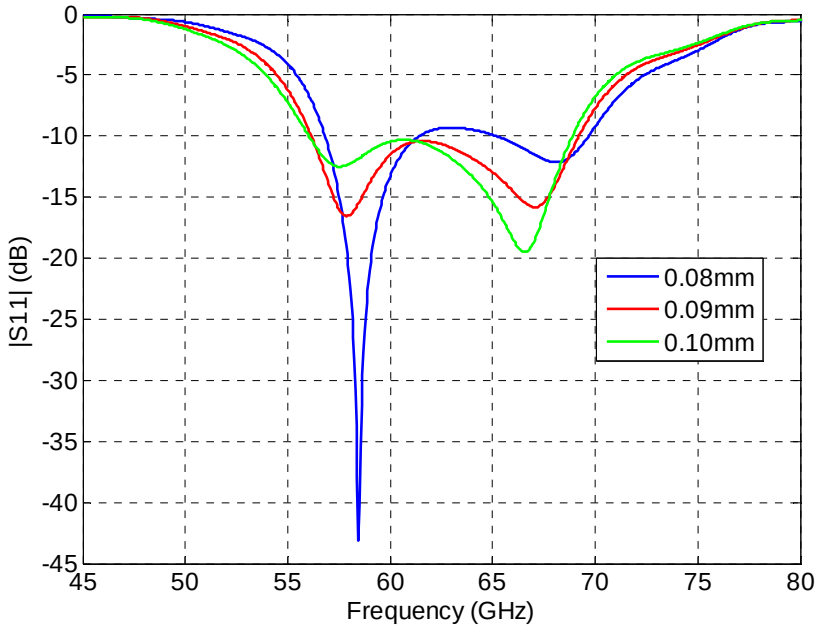

Figure 5.20: S_{11} sensitivity Vs l_2 (side arm width)

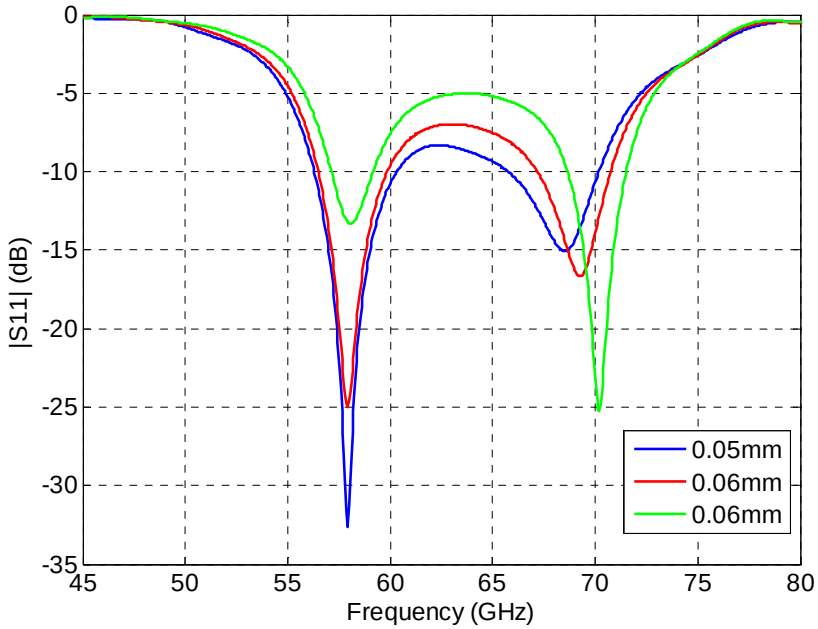

Figure 5.21: S_{11} sensitivity Vs w_2 (center arm width)

Substrate height

The sensitivity of the characteristics with respect to the fabrication tolerance on the substrate height is shown in Figure 5.22. The substrate (DP-943) normally has thickness of 104µm after co-firing. The tolerance on this value is ±4µm. The thickness of the substrate layer is varied between 100 to 112µm. It can be inferred from the graph that the bandwidth characteristics is maintained till a value of 108µm. The variation for a thickness of 112µm is quite large. If the fabrication tolerances are within the ±4µm value, then the characteristics can still be maintained for minor deviations in fabrication. The effect of the variation in the substrate thickness on the radiation characteristics was bear minimal and hence not presented here explicitly.

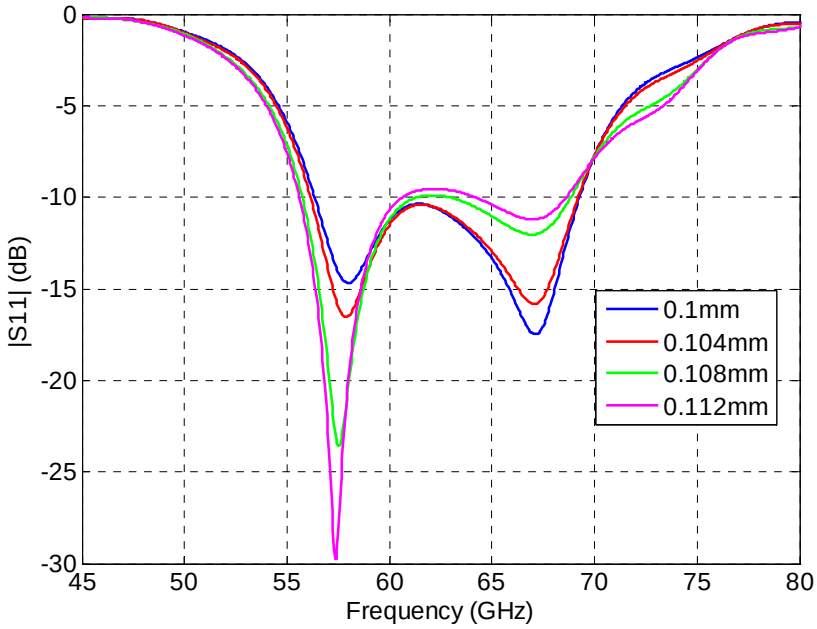

Figure 5.22: S_{11} sensitivity on the substrate height variation (tolerance)

Feed pin diameter and separation

The feed pin dimensions needs to be fabricated precisely in order to obtain proper bandwidth and radiation characteristics. The sensitivity carried out was done in terms of the feed pin diameter (d) and separation between the centers of the feed pins (S). The results obtained for various feed pin diameters and separations are shown in Figure 5.23(a) & (b).

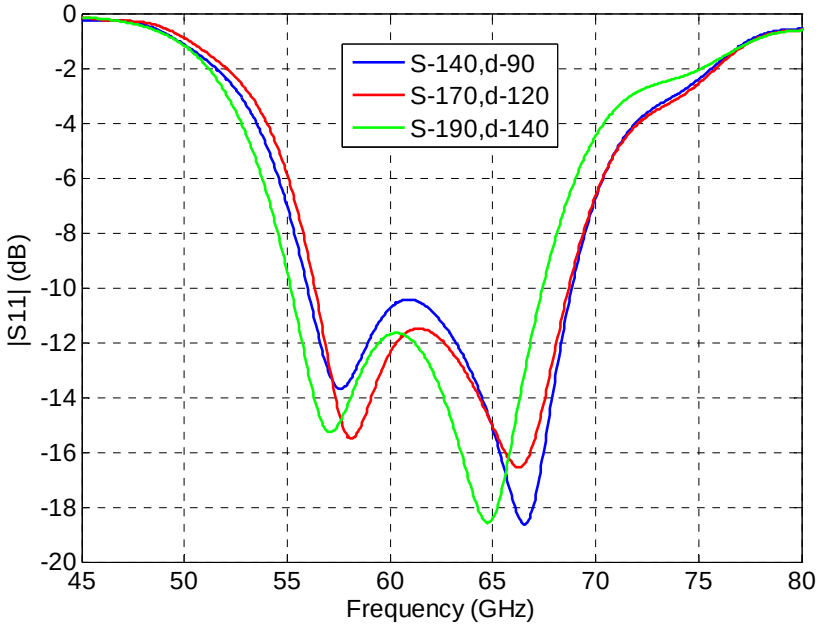

Figure 5.23(a): Sensitivity Vs feed pin dimensions and separation

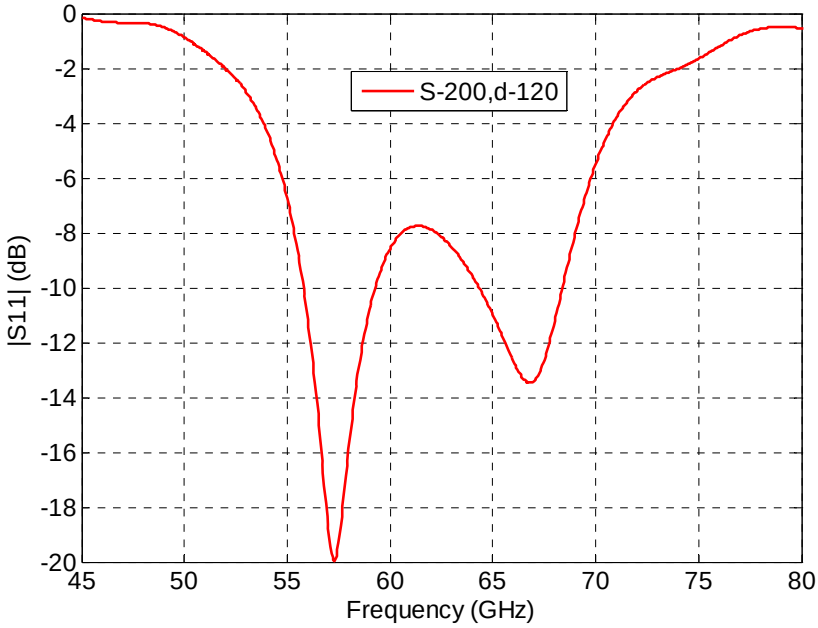

Figure 5.23(b): Sensitivity Vs feed pin dimensions and higher separation

NOTE: All dimensions specified in Figure 5.23(a) & (b) are in terms of micrometer (μm)

In general, the characteristics are retained if the feed pin diameter (d) is less than 140μm and the separation scaled with the following relation:

Separation between feed pin centers (S) = aperture center arm width (w_2) + d + 10μm

The bandwidth shifts more to the left (Figure 5.23(a)) for a diameter of 140μm, which is not a favourable characteristic. Hence, the diameters have to be kept less than this value for ensuring proper bandwidth coverage. If the original diameter of the feed pins as presented in Table 5.2, presents a fabrication constraint, then values of 100μm-120μm can be considered as alternatives.
The plot in Figure 5.23(b) shows effect of having a separation which disrupts the entire bandwidth characteristic.

5.7 Critical dimensions of the antenna

The critical dimensions of the antenna can be best explained by classifying them according to their impact on the main characteristics. With respect to this thesis project, the dimensions can be classified as critical dimensions with respect to the bandwidth characteristics, radiation characteristics and other characteristics. The summary of this analysis is presented in this section.

Bandwidth: The critical dimensions with respect to the bandwidth requirement are the patch dimensions and the substrate height. It is clear from Section 5.3.1, which presents the optimization of the patches that the frequencies at which the resonances occur is strongly influenced by the patch dimensions. The substrate heights play an important role in determining the bandwidth value itself. It is very evident from Section 5.3.4, that an increase in the substrate height by a layer completely disrupts the bandwidth characteristics.

Radiation characteristics: The critical dimensions in this case are the dimensions of the grided plane and the substrate. An increase in the dimension of the grided plane will reduce the amount of backward radiation thereby enhancing the front-to-back ratio. But an increase in the dimensions of the plane will make the beam narrower as well. So a trade-off needs to found out for its dimensions.
The dimensions of the substrate are kept bigger than that of the grided plane in order to have better contact between layers and also to keep the ratio of the non-metallised to the metallised regions higher. But increasing the dimensions of the substrate arbitrarily will result in unnecessary radiation from the substrate itself and hence will distort the pattern too. In this case the dimensions as given

in Table 5.2 are maintained as these dimensions helped in keeping the substrate larger than the grided plane and also to maintain regular radiation patterns over the operational bandwidth.

Other characteristics: The shape of the patch plays a vital role in the beamwidth which is possible in the E and H-planes. The design presented makes use of a rectangular patch which results in a comparatively narrower beam (~70-75 degrees) in the H-plane as the patch width is smaller than its length. An alternative which makes use of a square patch can be used, but will result in increased levels of cross polarization. This was also the main reason for avoiding the square patch in the design presented in this thesis.

5.8 Realization of the Antenna in LTCC

The antenna will be manufactured in the LTCC fabrication unit at TU-Ilemenau. The simulated antenna's dimensions are within the realization limits of the fabrication process. This helps in avoiding unknown complications in the fabrication process. The dimensions of the substrate are kept larger than that of the intermediate ground plane in order to increase the percentage of non-metallised region compared to the metallised region, a fact which is very important during the LTCC fabrication process. This helps in better contact between the layers and hence helps to keep the layered structure intact. A three dimensional view of the antenna is shown below in Figure 5.24.

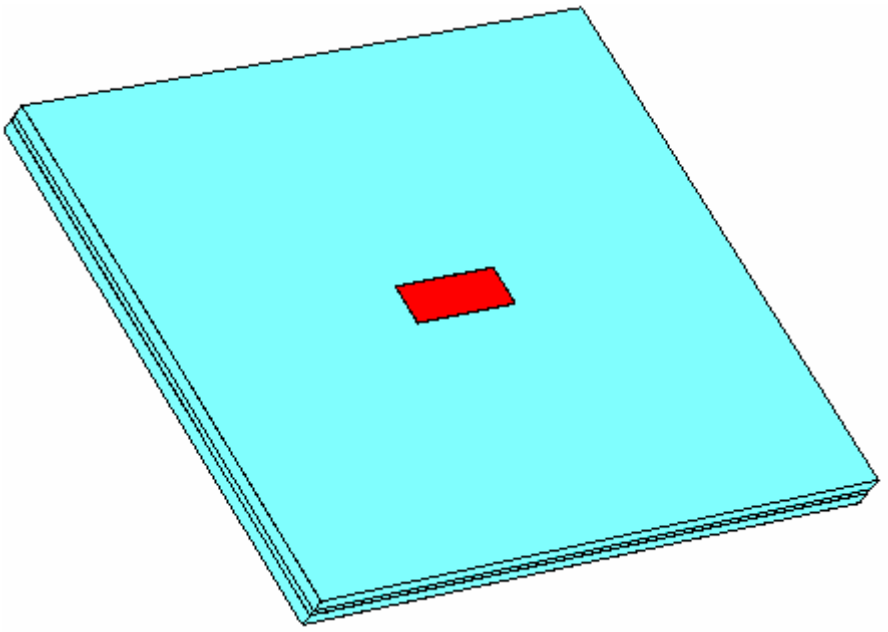

Figure 5.24: Three dimensional view of the antenna

6

CONCLUSIONS

In this thesis a UWB antenna operating in the mm-wave frequencies has been designed. The antenna satisfies the requirements of the project in terms of operational bandwidth, radiation characteristics, size and the inclusion of a differential feeding structure. A study on three possible candidate antennas was carried out, the results of which aided in the selection of the type of antenna which was apt for the project's requirement. Further, the analysis of the three candidate antennas provided useful insights into their feasibility in LTCC technology and also the operational characteristics which can be expected from them.

The design of an H-shaped Aperture Coupled Stacked Patch Antenna with differential feeding is presented in this thesis. The antenna achieves an operational bandwidth of nearly 13GHz and a front-to-back ratio (FBR) of around 13dB at the mm-wave frequencies with the proposed differential feeding structure and substrates with very high dielectric permittivity (ε_r=7.4). These factors account for the novelty in the design. The antenna is to be realised in LTCC technology at TU-Ilmenau's fabrication unit.

In addition to this, two more designs of the Stacked Patch antenna configurations are also presented in this report. The first design shows that a 17% bandwidth can be achieved through a single pin feed structure. It is evident from the second design that achieving wide bandwidths of operation with the use of Microstrip feeding network will in itself be a challenging task. The configuration also

suffers from bad radiation characteristics. Similar configurations can be avoided to expedite future design processes.

Suggestions and scope for improvement

The use of optical imaging for each layer in the LTCC fabrication process can help in providing a good insight into the discrepancies between the simulated and realised dimensions of the components of the configuration. This can aid is analysing the reasons for the deviation in the behaviour between the simulated and the experimental measurements.

Scope for improvement: The antenna design presented in this thesis has certain shortcomings. The antenna does not cover about 1GHz of the bandwidth from 60-70GHz. This can be achieved through some fine tuning, if necessary. Another issue is the optimization of the gain characteristics. As presented in Section 5.4, the gain of the antenna decreases slightly as the frequency increases, which is contrary to the normal behaviour. This can be changed by re-optimising the antenna with respect to the radiation characteristics. However, this process will not be extensive. The front-to-back ratio can be increased further by increasing the dimensions of the ground plane, if the size of the antenna is not a constraint. But an increase in the dimensions of the ground plane will also result in a narrower radiated beam. Also, the beamwidth of the antenna is less in the H-plane (~75 degrees). This can be increased by increasing the width of the rectangular patches or by using square patches. But, as mentioned in Section 5.3.1, the increase in the width of the patches shifts the resonances to lower frequency bands and also the use of square patches results in higher cross polarizations. An alternative solution which avoids these problems can be employed to get wider beamwidth in the H-plane. Finally, although the antenna is well suited for implementing in arrays due to its planar profile and good characteristics, the antenna need to be tested and modified slightly with respect to the requirements of the array before it can be used in the array arrangement.

Future work

The next step in the RADIOTECT project will be the implementation of the Stacked Patch antenna in an array configuration. The noise radar which will be used for the through-dress imaging requires an array for the scanning purposes. The antenna realised in the project has a good phase characteristic and is also a planar structure. Both these characteristics are very pivotal for an antenna array. Hence, the Stacked Patch antenna presented in this thesis can be readily used for an array implementation.

EUMW 2008

The design of the novel H-shaped Aperture Coupled Stacked Patch Antenna with a Differential Feeding structure, presented in this thesis report has been accepted to the *38th European Microwave Week*, to be held in October 2008 at Amsterdam.

Stacked Patch antenna with single feed at mm-wave frequencies- The design of a Stacked Patch antenna with a single pin feed as presented in Chapter 4, is currently being compiled as another publication for a suitable conference in the next few months.

APPENDIX A

NUMERICAL METHODS

A brief description of the numerical Electromagnetic solvers, which were used for the modeling and theoretical analysis of the antenna modules is presented in this section

A.1 FEKO

The core of the program of FEKO [26] is based on the Method of Moments (MoM). The MoM is probably the most widely used numerical technique. In MoM, the radiating/ scattering structure is replaced by equivalent currents. These are normally surface currents. The surface current is discretized into wire segments and/or surface patches. A matrix equation is then derived, representing the effect of every segment/patch on every other segment/patch. This interaction is computed using the Green function for the problem. The boundary condition is then applied to all the interactions, yielding a set of linear equations. The solution of this linear system yields the current on each segment/patch. The resulting matrix which must be factored is fully populated, with complex valued entries. Typical matrix dimensions range from some hundreds for small antennas to several thousand, depending on the upper limits imposed by the computational limitations. Once the current distribution is known, further parameters such as the near field, far field, scattering, directivity or input impedance of the antenna can be obtained.

Typically, the MoM has been applied in the frequency domain, i.e. single frequency, or monochromatic, sinusoidal excitation, with an $e^{j\omega}$ convention assumed. The working variables are thus complex valued, with a magnitude and phase, as for phasor analysis.

When we deal with usage of MoM, the basic step is the discretization of the geometry into smaller elements. The simplest and the most basic approach involved the splitting of the geometry into smaller square patches. But, the usage of a triangular patch for two dimensional structures served as

a better approximation compared to the one with the square patch. FEKO makes use of the same idea. An important consequence of this is that the physical parameter Js which is approximated is now two dimensional and hence the basis function must also incorporate this. A method devised by Rao, Wilton and Glisson is the most widely used basis function for the triangular patch method. It was proved later that this basis function is similar to the one used in the finite element analysis.

The basis function is based on many features, the most important of which is that the basis function is vector in nature, which means that the individual components of the current density J, can only be recovered with some manipulation. The essence of the idea is to enforce current continuity over an edge of the patch. The interpolation function for this is defined accordingly.

The existence of a coordinate system called the simplex coordinate system makes the study of the interpolation functions on triangles much simpler and is also widely used in the finite element analysis. The simpler current interpolation is shown in Figure A.1.

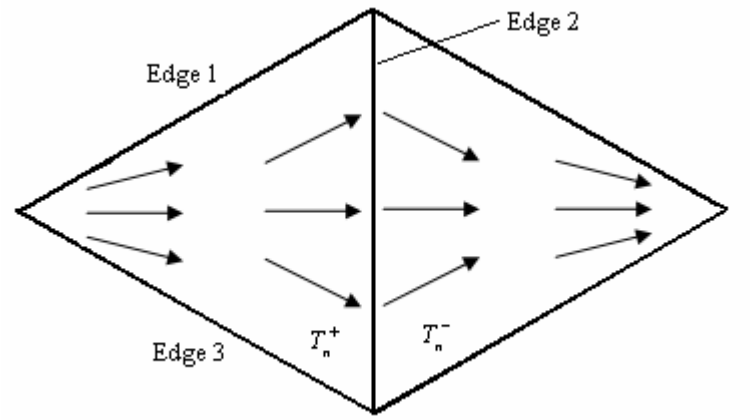

Figure A.1: A vector plot of the RWG basis function

It should be noted that this basis function has normal component to the upper or the lower sides of either of the triangles. The component is normal only to the central edge. The assumption done here is that the current crossing the shred edge is interpolated in a tangential direction and interpolated as a constant normal to the edge. The latter value is called the degree of freedom which is associated with the basis function. Hence the current associated with the edge is approximated as $\vec{J}_n(\vec{r}) \approx I_n \vec{f}_n(\vec{r})$. All the terms are expressed in terms of the local coordinates on the triangle and the conversion to the Cartesian coordinate systems is done using the simplex coordinates. For the currents across the other edges, an additional basis function is defined on either of the triangles, which results in three basis functions on the whole. These three functions have three associated unknowns, which are normal components of the current on each edge. Within the element it should

be arrived that the total current is approximated by the sum of these three basis functions. With the edges as defined in Fig.1, the total current on the triangle is given by (approximate value)

$$\vec{J}_n(\vec{r}) \approx I_1 \vec{f}_1(\vec{r}) + I_2 \vec{f}_2(\vec{r}) + I_3 \vec{f}_3(\vec{r}), \qquad \forall \vec{r}\, in T_n^+ \qquad (1)$$

We can see that the basis functions carry the vector information; the unknown for which the code solves (I_1, I_2, and I_3) are just scalars.

A.2 Computer Simulation Technology (CST)

The main 'general-purpose' algorithms are based on surface discretization or volume discretization. Finite Integration Technique (FIT), which is used in CST, is based on the latter volume discretization method. The **F**inite **I**ntegration **T**echnique (FIT) was developed around thirty years ago and has grown into a very general approach to solve Maxwell's equations. It generates exact algebraic analogous to Maxwell's equations, which guarantees that the physical properties of fields are maintained in the discrete space, and lead to a unique solution [27]. The basic idea of FIT is that it offers a geometric description of discrete electromagnetic problems without specifying a priori the type of the "discretization method". For instance, one may implement into FIT the local approximation method of Finite Elements as well as the classical FIT approach using voltages along edges and fluxes through surfaces. In the very first step, the problem has to be discretized in either coordinate meshes or tetrahedral meshes, as shown in Figure A.2.

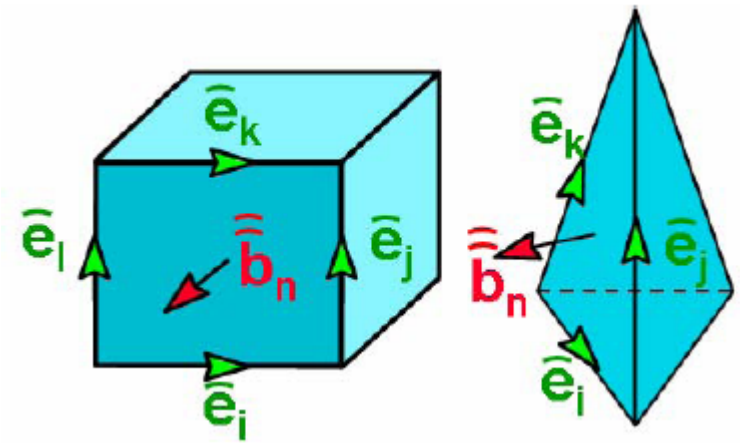

Figure A.2: FIT allocation of voltages and fluxes along edges and through surfaces, respectively

The next step is to solve the first Maxwell's equation for the elementary cells for all surfaces:

$$\oint_{\partial A} E.ds = -\iint_{A} B.dA \qquad (2)$$

The result of the integration of 4.1 over the cell of the cube using the notations of Figure A.2, reads

$$e_l^{'} + e_k^{'} - e_j^{'} - _i^{'} = -d(b_n^{''})/dt \qquad (3)$$

In case of the tetrahedral cell the summation on the left hand side has one component less than in 2

$$e_l^{'} + e_k^{'} - e_j^{'} - _i^{'} = -d(b_n^{''})/dt \qquad (4)$$

The single hyphen on top of the electric voltages denotes the fact that this quantity was integrated along a line; the hyphen dash denotes quantities that are integrated over areas. Once all unknown elements of all surfaces of the entire mesh are collected in long vectors, one may write the discrete equivalent of the Maxwell equation 1, in a simple matrix form as:

$$\underbrace{\begin{pmatrix} . & . & . & . \\ 1 & 1 & -1 & -1 \\ . & . & . & . \end{pmatrix}}_{C} \underbrace{\begin{pmatrix} e_i^{'} \\ e_j^{'} \\ e_k^{'} \\ e_l^{'} \end{pmatrix}}_{e^{'}} = \underbrace{-\frac{d}{dt}\begin{pmatrix} . \\ b_n^{''} \\ . \end{pmatrix}}_{-b^{''}} \qquad (5)$$

The "curl"-matrix **C** has only elements 0, +1 or -1. In an almost identical way one may write down the second Maxwell equation on a dual grid for the quantities respectively. Similarly, the remaining Maxwell's equations may be transformed into a discrete set, so that one finally obtains the so-called **M**axwell's **G**rid **E**quations produced by the FIT approach as:

$$\oint_{\partial A} \vec{E}.\vec{ds} = -\int_{A} \frac{\partial}{\partial t} \vec{B}.\vec{dA} \leftrightarrow C\,\bar{e} = -\frac{d}{dt}\bar{\bar{b}} \qquad (6)$$

$$\oint_{\partial A} \vec{H}.\vec{ds} = -\int_{A} \left(\frac{\partial \vec{D}}{\partial t} + \vec{J} \right).\vec{dA} \leftrightarrow \bar{C}\,\bar{h} = \frac{d}{dt}\bar{\bar{d}} + \bar{\bar{j}} \qquad (7)$$

$$\oint_{\partial V} \vec{B}.\vec{dA} = 0 \leftrightarrow S\,\bar{\bar{b}} = 0 \qquad (8)$$

$$\oint_{\partial V} \vec{D}.\vec{dA} = \int_{V} \rho dV \leftrightarrow \bar{S}\,\bar{\bar{d}} = q \qquad (9)$$

It is worthwhile to note here that this set of equations is **exact** and has no discretization error involved. The inexact part comes into the equation only when the material relations are brought into a discrete form. The algebraic structure of the discrete material relations is independent of the method for the local field approximation and results in

$$\vec{D} = \varepsilon . \vec{E} + \vec{P} \leftrightarrow \bar{\bar{d}} = M_{\varepsilon} \bar{e} + \bar{\bar{p}} \qquad (10)$$

$$\vec{B} = \mu . \vec{H} + \vec{M} \leftrightarrow \bar{\bar{b}} = M_{\mu} \bar{h} + \bar{\bar{m}} \qquad (11)$$

$$\vec{J} = \kappa . \vec{E} \leftrightarrow \bar{\bar{j}} = M_{\kappa} \bar{e} \qquad (12)$$

Furthermore, discrete fields are not calculated exactly on a real computer due to round off error or other numerical effects. These equations are thus an ideal tool to control a posteriori the quality of computed results. The method not only works for virtually any kind of mesh, be it tetrahedral, non-orthogonal hexahedral or any other coordinate grid, but it may also employ various discretization methods in the classical language when modeling the material relations locally, including edge elements as used in many Finite Element approaches.

The generality of the FIT approach yields an ideal base for implementations in computer codes. Starting almost 30 years ago, a long series of codes has been written by several authors [28, 29 and 30] for many different applications ranging from statics over quasi-statics to high frequency problems. Computer codes based on FIT have become a routine tool in industry and research.

As FIT offers frequency domain, time domain explicit and implicit, modal analysis and model order reduction, one can often solve one and the same problem with completely different algorithms. This gives one not only the possibility to choose the most efficient algorithm, but also offers independent results for cross verification.

APPENDIX B

NUMERICAL APPROXIMATIONS

Approximate EM problem

The EM problem at hand has certain complexities which require the approximation of the AEM problem in order to be theoretically analysed with the numerical solvers. The modifications which are carried out with respect to the antenna's design configuration are presented in this section. The reasons and validations for the approximations are also mentioned in the sections below.

Dielectric constant

The dielectric substrate which is used for the design of the antenna has a dielectric permittivity of 7.4. This value is assumed to constant over the entire frequency band of operation.
Validity: This assumption is valid as the substrate which will be used to fabricate the actual antenna is DP-943 [31], which has an almost stable dielectric permittivity even above 60GHz.

Dielectric loss tangent

The dielectric loss tangent of the substrate is assumed to be equal to 0. This assumption is valid as the loss tangent of the DP-943 substrate is equal to 0.002 for practical applications.

Metal patches

The metal patches and cylinders are assumed to be perfectly conducting materials (PEC). The thickness of the metal patches used is equal to 0.009mm or 9μm. This is equal to the thickness of the patches which are used in actual fabrication processes.

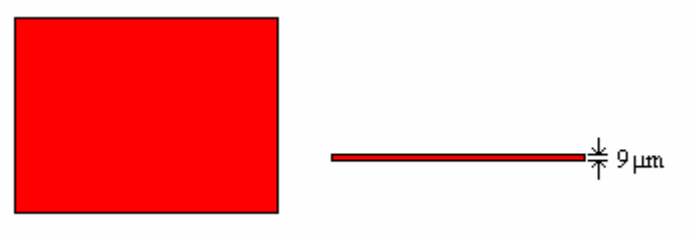

Figure B.1: Metal patch and its thickness

Feeding structure

A differential feeding structure is required to feed the antenna. The feeding structure helps in the achieving direct contact with a MMIC which has a differential output. The output pins from the MMIC is with the GSSG (Ground-Signal-Signal-Ground) configuration. This means that the center points (SS) provide the necessary feeding with opposite polarities. A differential feeding structure similar to the one shown in the figure below is used for providing a differential feeding to the antenna in the simulation process.

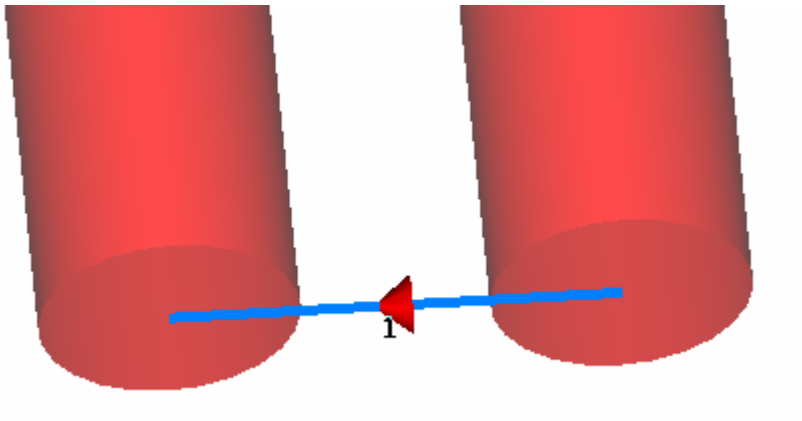

Figure B.2: Feeding structure used for the numerical analysis

Validity: The feeding structure shown above is implemented using the "*discrete port*" option in CST. This is done to mimic the actual GSSG output configuration of the MMIC. The use of the discrete port provides excitation with opposite polarity between the two feed pin cylinders. In actual measurements the two feed pins can be kept in direct contact with the SS points in the MMIC's GSSG output port. Thus it can be stated that using this type of feed option, it is possible to mimic the actual feeding provided from the MMIC.

Grided plane

The part of the ground plane near the aperture slot is maintained as a continuous plane while the grid slots are made in the remaining part of the ground plane. The length and width of the grid slots are kept equal to $\lambda_d/8$, which in this case is equal to 1.7/8mm≈0.22mm (λ_d =1.7mm). The value is chosen to keep the grid slots as large as possible to take into effect the maximum change in the characteristics due to the use of a grided plane. The usual size of the grid slots in the fabrication process is around $\lambda_d/12$ to $\lambda_d/8$. Hence, the approximated dimensions of the grid slots are well within the practical grid slot values of the LTCC process.

Effect of the size of discretization

The reflection coefficient characteristic for the antenna is shown in Figure B.3 for various mesh sizes of the segmentation procedure. It can be noticed that there are two resonances as a result of using the H-shaped aperture slot. The lengths of the center and the side arms of the aperture slot helps in attaining these two resonances. The lengths and widths of the lower and the top patch are varied to position the resonances in the desired frequency band of interest. The dimension of the lower is kept equal to 0.8x0.6mm and that of the top patch is kept equal to 1.65x0.6mm. Increasing the values of the dimensions of the patches will shift the resonances further to the left to lower frequencies. An opposite behaviour is noticed for a decrease in the dimensions. This variation is entirely physical as the resonant frequencies are dependent on the dimensions of the patches as they are scaled in terms of the dielectric wavelength (λ_d).

It can be inferred from the plot that a very low value of the mesh size ($\lambda_d/10$ to $\lambda_d/20$) provides a considerable variation in the behaviour. This can be a result of under-sampling. As the mesh size decreases further than $\lambda_d/30$ the variation is very minor. Mesh sizes below $\lambda_d/35$ values show a convergence in the characteristic and hence it can be concluded that having a mesh size below $\lambda_d/35$ would result in accurate numerical computations. However, decreasing the mesh size below $\lambda_d/50$ will not result in more accurate results and also might lead to numerical dispersion as a result of over sampling. It can thus be concluded that the variation in the S_{11} characteristics is purely numerical and not physical. The comparison in computational times for the different mesh sizes is presented in Table B.1. It can be seen from Table B.1, that the difference in the computational time and memory between $\lambda_d/35$ and $\lambda_d/50$ mesh sizes is quite significant. However, the difference in accuracy between the $\lambda_d/35$ and $\lambda_d/50$ mesh sizes in terms of S_{11} or the radiation characteristics is not significant. Hence, a mesh size equal to $\lambda_d/35$ is maintained for the simulation procedures. This falls

in the range which is usually kept for practical antenna designs where the value is kept in between $\lambda_d/30$ and $\lambda_d/40$ for good accuracy levels.

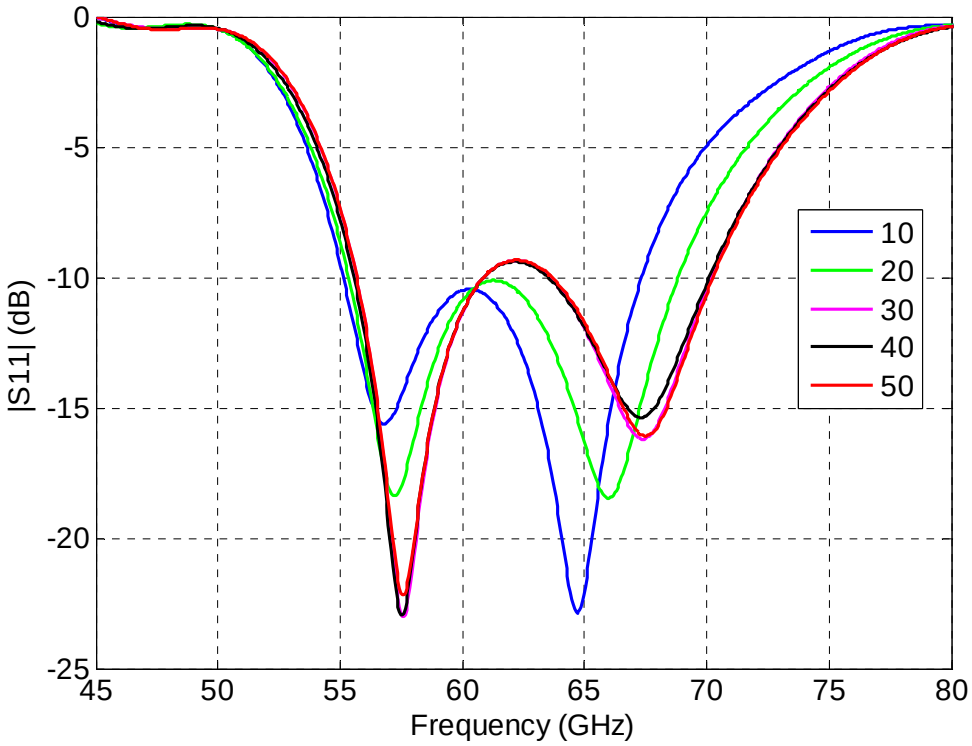

Figure B.3: Variation of reflection coefficient with mesh size

Mesh size	Computation Time	Memory
$\lambda_d/15$	5m 56s	98MB
$\lambda_d/35$	42m 16s	226MB
$\lambda_d/50$	2hrs 27m 6s	409MB

Table B.1: Comparison of computational resources for different mesh sizes

By keeping the mesh sizes equal to $\lambda_d/35$, the optimization procedure was continued to fine tune the S_{11} characteristics. It can be seen from Figure B.3, that the characteristics for mesh sizes below $\lambda_d/35$ have the central part of the curve slightly above the -10dB level. Also the resonances are not equally steep. By increasing the top patch length above 1.7mm, the whole curve is brought down below the -10dB level and also the resonances are "balanced". These factors helped in arriving at the final dimensions of the antenna.

Impact of the mesh size on the gain

The impact of the mesh size on the radiation characteristics is shown in Figure B.4. It can be seen that the impact of the mesh size on the pattern is very minimal. This is similar to the results presented in the lectures, where it was demonstrated that the gain pattern is not affected much by the discretization. As mentioned earlier a mesh size equal to $\lambda_d/35$ was maintained throughout the optimization process.

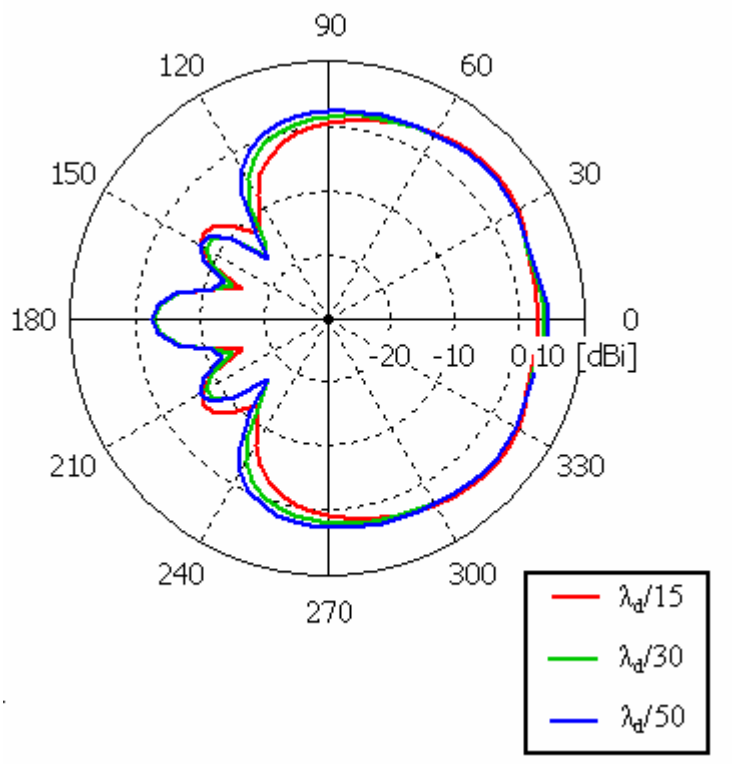

Figure B.4: Impact of the mesh size on the radiation pattern at 64 GHz

Summary of the analysis

It can be seen that the deviations in the S_{11} plot shown in Figure B.3 is entirely numerical and not physical. The resonances which are physically possible depend on the aperture slot and it can be seen from the same figure that there are two resonances in the frequency range of interest. Further, as mentioned above, the resonant frequencies depend on the dimensions of the lower and the top patches. As we decrease the mesh size more accurate plots are obtained, but only with two resonances. This can be attributed only to the numerical properties of the solver and not anything physical concerned with the configuration of the antenna. Also, the use of the grided plane does not affect the S_{11} and the radiation characteristics to a considerable level. From the results obtained it is evident that apart from the small change in the S_{11} characteristics induced by the grided plane, other

deviations in the results which might indicate physical discrepancies are not present. The impact of the mesh size on the radiation pattern is also found to be very minimal, which is primarily due to the fact that the far field is practically insensitive to the mesh size variations. The antenna is realizable with the dimensions as presented in Table 5.2. This makes the design of the antenna more practical apart from being simple. Hence, the approximations presented in this chapter are justified with respect to the final goal of this thesis.

APPENDIX C

DUPONT DP-943 DATASHEET

The characteristics of the substrate used for the fabrication process, DuPont's DP-943 [31], are presented in this section via the table shown below. The substrate is mainly chosen for its stable permittivity value at 60GHz and also due to its low loss tangent (tanδ=0.002).

Typical Properties of DuPont DP-943	
Physical	
Unfired thickness (μm)	127±9(943P5)
X, Y Shrinkage (%)	9.5±0.3
Z Shrinkage (%)	10.3±0.5
TCE (25-300 ^{o}C), ppm/ ^{o}C	6.0
Density (g/cm^3)	3.2
Camber, inch/inch	<0.001
Surface roughness (μm)	0.64
Thermal conductivity, W/m-k	4.4
Flexural strength, MPa	230
Young's modulus, GPa	150
Poisson's ratio	0.24
Electrical	
Dielectric constant @ 40GHz	7.4
Loss tangent @ 40Ghz	0.002
Breakdown voltage V/μm	$>10^{12}$
Insulation resistance at 100 VDC, Ω	>1100/25

Table C.1 – Characteristics of DP-943

REFERENCES

[1] Hans Gregory Schantz, "Introduction to Ultra Wideband Antennas", *Invited Talk, IEEE IWUWBS/UWBST,* 2004.

[2] Hans Gregory Schantz, "Dispersion and UWB Antennas', *Plenary Talk, IEEE UWBST,* 2003.

[3] M.A.Peyrot-Solis, G.M. Galvan Tejada, H.Jardon-Aguilar, "State of the Art in Ultra-Wideband Antennas", *2nd International Conference on Electrical and Electronics Engineering (ICEEE),* p.p.101-105, 2005.

[4] Y.Kim, D.H. Kwon, "CPW-fed Planar Ultra Wideband Antenna having a Frequency Band Notch Function", *Electronic Letters,* vol. 40, No.7, p.p.403-405, 2004.

[5] Antti Laminen, "Design of millimeter-wave antenna on LTCC substrates", *Masters Dissertation, Helsinki University of Technology,* 2006.

[6] Ingo Wolff, "Design and Technology of Microwave and Millimeter LTCC Circuits and Systems", *International Symposium on Signals, Systems and Electronics, ISSSE 2007.*

[7] P.J.Gibson, "The Vivaldi Ariel", *presented at 9th European Microwave Conference*, p.p-101-105, 1979

[8] Yan Venot, Karin Schuler, Werner Wiesbeck, "Tapered Slot Antenna for LTCC Multilayer Substrate Integration in mm-Wave Applications"- *Institut Fur Hochstfrequenztechnik und Electronik*, Karlsruhe University.

[9] G.Brezezina, L.Roy and L.MacEachern, "Planar Antennas in LTCC Technology with Transceiver Integration Capability for Ultra-Wideband", *IEEE Trans. on MTT*, vol. 54, No.8, p.p. 2830-2839, 2006.

[10] Ramakrishna Janaswamy, Daniel H. Schubert, "Analysis of the Tapered Slot Antenna", *IEEE Transactions on Antennas and Propagation*, 1987.

[11] A. V. Vorobyov, A. G. Yarovoy, P. Aubry, L. P. Ligthart, "Backside Shield Optimization for UWB Antennas"- *International Research Centre for Telecom and Radar, Delft University of Technology*, Netherlands.

[12] S.D.Targonski, R.B.Waterhouse, and D.M.Pozar, "Design of Wide-Band Aperture- Stacked Patch Microstrip Antennas", *IEEE Transactions on Antennas and Propagation*, vol. 46, 1998.

[13] A.Panther, A.Petosa, M.G.Stubbs and K.Kautio, "A Wideband Array of Stacked Patch Antennas Using Embedded Air Cavity in LTCC", *IEEE Microwave and Wireless Components Letters*, vol. 15, p.p. 916-918, 2005.

[14] Woojin Byun, Ki Chan Eun, Bong Soo Kim, Kwang Sun Kim, Myung Sun Song, "Design of 8x8 Stacked Patch Array Antenna on LTCC Substrate Operating at 40GHz Band" - *Advanced Radio Technology Department, Electronics and Telecommunications Research Institute*, Korea.

[15] Rob.B.Waterhouse, "Design of Probe-Fed Stacked Patches", *IEEE Transactions on Antennas and Propagation*, vol. 47, p.p.1780-1784, 1999.

[16] E.Tentzeris, R.L.Li, K.Lim,, M.Maeng, E.Tsai, G.DeJean and J.Laskar, "Design of Compact Stacked Patch Antennas on LTCC Technology for Wireless Communication Applications", *IEEE Transactions on Advanced Packaging*, vol. 27, p.p. 581-588, 2004.

[17] J.A.G.Akkermans, M.C. van Buerden and M.H.A.J.Herben, "Design of a Millimeter Wave Balanced-Fed Aperture Coupled Patch Antenna", *Proc. EUCAP 2006*, Nice, France.

[18] Quan Xue, Xiu Yin Zhang and Ching-Hong K.Chin, "A Novel Differential-Fed Patch Antenna", *IEEE Antennas and Wireless Propagation Letters*, vol. 5, p.p. 471-474, 2006.

[19] Shi-Chang Gao, Le-Wei Li, Mook-Seng Leong and Tat-Soon Yeo, "Wide-Band Microstrip Antenna With an H-Shaped Coupling Aperture", *IEEE Transactions on Vehicular Technology*, vol. 51, p.p. 17-26, 2002.

[20] Ee Lee, Kin Meng Chan, Peter Gardner and T.E. Dodgson, "Active Integrated Antenna Design Using a Contact-Less, Proximity Coupled, Differentially Fed Technique", *IEEE Transactions on Antennas and Propagations,* vol. 55, 2007.

[21] David. M. Pozar, "A Review of Aperture Coupled Microstrip Antennas: History, Operation, Development and Applications", *University of Massachusetts, Amherst*, 1996

[22] Garg, Bhartia, Bahl, Ittipiboon, "Microstrip Antenna Design Handbook", Artech House Inc, 2001.

[23] Gildas P.Gauthier, Jean-Pierre Raskin, Gabriel Rebeiz, "A 94 GHz Aperture-Coupled Micromachined Microstrip Antenna", *University of Michigan, Ann-Arbor*, *USA*, 2005.

[24] H.S.Shin and N.Kim, "Wideband and High Gain One-Patch Microstrip Antenna Coupled with H-Shaped Aperture", *Electronic Letters*, vol. 38, p.p. 1072-1073, 2002.

[25] Nicolaos G.Alexopoulos, Pisti B. Katehi, D.B. Rutledge, "Substrate Optimization for Integrated Circuit Antennas", *IEEE Transactions on Microwave Theory and Techniques,* vol. MTT-31, p.p. 550-557, 1983.

[26] David B. Davidson, "Computational Electromagnetics for RF and Microwave Engineering", *Cambridge University Press, 2005*.

[27] T.Weiland and Irina Munteanu, "State of The Art and The Future in Modelling RF Components", *Pro .EUCAP 2006*, Nice, France.

[28] Wieland T, "On the Unique Numerical Solution of Maxwellian Eigen-value Problems in Three Dimensions", *Particle Accelerators*, vol.17, p.p. 227-242, 1985.

[29] Weiland T, TBCI and URMEL, "New Computer Codes for Wake Field and Cavity Mode Calculations", *IEEE Transactions on Nucl. Sci.* vol. NS-30, p.p. 2489-2491, 1983.

[30] Van Rienen, Weiland T, "Triangular Discretization Method for the Evaluation of RF Fields in Cylindrically Symmetric Cavities", *IEEE Trans. Mag.* Vol. MAG-21, p.p. 2317-2320, 1985.

[31] DuPont Microcircuit Materials: 943 low-loss green tape datasheet. [Online]. Available: http://www.dupont.com/MCM/en_US/PDF/datasheets/943.pdf.